



Universidad Autónoma de San Luis Potosí
Facultad de Ciencias



Optical anisotropy study in coupled quantum wells, a novel source of undisturbed systems

Doctoral Thesis in Applied Sciences
submitted by:

Oscar Ruiz Cigarrillo

Supervisors:

Dr. Luis Felipe Lastras Martínez

Dr. Edgar Armando Cerda Méndez

SAN LUIS POTOSÍ, S.L.P. MÉXICO
JANUARY 2022

CONTENTS

List of Figures	II
List of Tables	V
Abbreviations	VI
List of codes and packages	VII
Symbols	VIII
1 Physical Background	1
1.1 Semiconductor Bandstructure	2
1.1.1 Valence and Conduction Bands	3
1.1.2 Excitons	8
1.2 Semiconductor Low-Dimensional Structures	9
1.2.1 Quantum wells	10
1.2.2 Preliminary approach of Quantum Confinement effect in QWs	11
1.3 Summary	14
2 Physical model	15
2.1 The Symmetry Context	16
2.1.1 The symmetry and the Band Structure	19
2.2 Symmetry breaking in Semiconductor Structures	21
2.3 General revision of numerical methods	22
2.3.1 Finite Difference Method	22
2.4 Structural Parameters	22
2.5 Anisotropy model in CQWs	22
3 EXPERIMENTAL DETAILS AND RESULTS	23
3.1 Samples Description	24
3.2 Spectroscopy: Experimental setups and experimental results	27
3.2.1 Photoluminescence Spectroscopy (PL)	28
3.2.2 Photoreflectance spectroscopy (PR)	36
3.2.2.1 Excitonic effects	42
3.2.2.2 The PR summary	51
3.2.3 Reflectance Anisotropy Spectroscopy (RAS)	51
4 CONCLUSIONS	53
Bibliography	54

LIST OF FIGURES

1.1	Band energy diagram for insulators (left), semiconductors (center) and metals (right). The principal difference is the gap energy, for insulators this is longer than semiconductors, although in semiconductors gap energy depends on materials, finally in metals doesn't exist gap energy instead exist an overlap bands characterize these. Dashed line determine Fermi's level.	4
1.2	GaAs crystal lattice, where each sublattice correspond of each atom species Ga and As.	5
1.3	Band structure of GaAs, (a) shows the zoom around of Γ to denote the direct band gap and the electrons energy needed to jump from valence to conduction band. (b) denotes the two directions to dispersion of the bands corresponds to Brillouin zone: $\Gamma \rightarrow X$ and $\Gamma \rightarrow L$. [1]	6
1.4	Two typical transitions for GaAs near $\mathbf{k} = 0$. The first one correspond to the heavy-hole and second one to the light-hole.	7
1.5	Qualitative scheme of exciton creation in GaAs as direct gap.	8
1.6	General scheme of GaAs/ $Al_xGa_{1-x}As$ heterostructure, at top show the scheme of atomic arranged of this heterjunction, the dashed lines are the matched between two dissimilar materials. In bottom shows the band-edge profile.	9
1.7	Heterostructures from bulk (3D), to Quantum Wells (2D), Quantum Wires (1D) and Quantum Dots (0D).	11
1.8	GaAs/ $Al_xGa_{1-x}As$ Single Quantum Well	12
1.9	General scheme of typical Schrödinger's equation solutions to one-dimensional potential as (a) where the Eigenenergies of both electron and holes are denoted with same color depending on n value.(b) It's plot, of the subbands in the same case of (a) to both particles.	13
2.1	(a) GaAs crystal structure in “real space”, this region is known as <i>unit cell</i> , into that with dashed line is denoted the primitive cell. This lattice is well-defined by the vectors \mathbf{a} , \mathbf{b} and \mathbf{c} , these vectors are defined as the basis vectors. In (b) is schematized the GaAs crystal structure in \mathbf{k} -space, also known as <i>reciprocal space</i> .	17
3.1	GaAs substrate growth direction	24
3.2	AlGaAs superlattice	25
3.3	Processes that occur inside a solid in the light-matter interaction phenomena	27
3.4	PL Scheme	29

3.5 Subfigure (a) shows PL experiments of the samples M4_3171 , M4_3172 and M4_3226 , where show spectra and results measured at 14K. Plots in how the comparison between these samples, where clearly can see the relative intensity among in each experiment. In (b) it can be seen each PL spectra with the respective direct transitions numerically calculated, hh1 and lh1 indicates the first energy level that corresponds to heavy- and light-holes respectively.	31
3.6 Absorption calculated as a function of sample depth, dashed lines closed the CQWs region, left: Figures 3.6(a) to 3.6(c),here the samples have $\text{Al}_x\text{Ga}_{1-x}\text{As}$ layers with different compositions $x = 0.15, x = 0.2$ and $x = 0.3$ this results in a change of refractive index then also expected in absorption. Right: Figures 3.6(d) and 3.6(f) and ?? these samples are equal in structure but change the width of one oM4a)f the QWs, therefore the absorption manifests more homogenous than the first three samples.	33
3.7 (a) Shows the PL spectra to samples M4_3140, M4_3521 and M4_3523, in this comparison is clear the shift between these in respect to first transitions. The relative change in width of one of the QW modify the energy transitions being the sample 3521 the lowest energy. (b) It is plotted each PL spectra result with the correspondent e1-hh1 and e1-lh1m transitions energies.	35
3.8 Scheme of the PR effect where it shows the carrier dynamics, in left can see the photoinduced changes by the laser is applied.	37
3.9 PR Scheme	38
3.10 PR experiments to samples: M4_3171, M4_3172 and M4_3226 at 30K. Arrows point to calculated transitions for each sample, the used laser wavelength was the same, which in PL experiments and the power used in each of these was 5mW. Dashed line point the GaAs substrate.	40
3.11 PR experiments to samples: M4_3140, M4_3141, M4_3521, M4_3522 and M4_3523 at 30K. Arrows point to calculated transitions for each sample, the used laser wavelength was the same, which in PL experiments and the previous PR experiments. Dashed line indicate the GaAs substrate, in these samples this transition is well located. The PR spectra of sample M4_3522 p-type doped (orange) is five times smaller than their correspond n-type, the sample M4_3521. The experiments in sample M4_3140 was performed at 2.5mW, then was multiply it by four in according to samples M4_3521 and M4_3523, in case of the sampleM4_3141 even if, was performed at a power = 5mW the result was 5 times smaller than sample M4_3521. The discussion about of this is explained in the text.	41

3.12 Comparison of : a) PR spectra of the 3521 (n-type) and 3522 (p-type) samples, the p-type sample is 5 times smaller than n-type sample. b) R spectra obtained at same time in each experiment, the arrows point to each direct transitions for two first confined energies. The line shape is practically the same in both spectra.	42
3.13 The PR comparison between samples M4_3521 (ACQWs-2) and M4_3523 (SCQWs), the electron wave function are plotted for each sample where, the SCQWs sample at top left and at top right to ACQWs sample. The top arrows pointed to forbidden transitions in ASQWs-1 sample, while the bottom arrows pointed to the direct transitions in both samples.	44
3.14 PR spectra of the ACQWs-1 sample designed as a function of slits aperture, where it can see the increase of peak resolution as decrease the aperture of slits.	45
3.15 The peak tends to height as increase the laser power, which also is very observable as a redshift.	46
3.16 Trions formation scheme in terms of band structure (a) in this case, the exciton is bound to an electron in the conduction band leading to a three-body system knew as negative trion \mathbf{X}^- . On the other hand, in (b) it presents the possible formation of \mathbf{X}^- due to a slight width of one in the CQWS, consequently, the narrow well transfers electrons through tunneling to a wide well, if it's calculated the wave functions of this structure, the wave functions have the characteristic of to be distributed asymmetrically as in the case of the applied electric field along z [2,3].	47
3.17 Results to self-consistently Schrodinger-Poisson equation, in order with down to top the n-type layer $\text{Al}_{0.15}\text{Ga}_{0.85}\text{As}$ doped ($6 \times 10^{18}\text{cm}^{-3}$) is increasing in width from 15nm, 75nm, 150nm to 300nm. The goal of this is to calculate in a general way the effects of the dopped layer, specifically due to the electric field induced by this. The strength of the field is expressed in kVcm units, although this magnitude si great, we assume that doesn't significantly, latter we explained this.	49
3.18 Band conduction profile $V(z)$ calculated by numerical solution of self-consistent Schrödinger-Poisson equation. The calculations were performed considering the width of the doped n-type 6×10^{18} layer with 600nm. The zoom inset shows the comparison between total potential calculated (blue) and when applied field $F \approx 1.2\text{kVcm}^{-1}$ (dotted magenta), where at around of CQWs zone are similar.	50
3.19	52

LIST OF TABLES

3.1	Table of samples description	26
3.2	Photo-cathodes, usually implemented in PD to the spectroscopy of semiconductors [4].	28
3.3	PL experimental parameters implemented in each sample, all experiments were carried about 14K and was used the same red (680 nm) laser diode. The measured parameters as a Wavelength step or number of acquisitions per step Wavelength were optimized as explains in the text.	30
3.4	Comparison table between experimental transitions obtained trough PL measures and numerical transitions calculated as explained in ??	36

ABBREVIATIONS

BZ	<i>Brillouin zone</i>
QS	Quantum Structures
QW	Quantum Well
CQWs	Coupled Quantum Wells
VB	Valence Band
CB	Conduction Band
SCQWs	Symmetric coupled quantum wells
ACQWs	Asymmetric coupled quantum wells
RAS	Reflectance Anisotropy Spectroscopy
PL	Photoluminiscense spectroscopy
PR	Photoreflectance spectroscopy
R	Reflectance spectroscopy
PRD	Photo-Reflectance Differential Spectroscopy
FDM	Finite differnce method
CCD	Charge coupled device
0D	Zero-dimensional
1D	One-dimensional
2D	Two-dimensional
3D	Three-dimensional
fcc	Face-centered cubic
<i>hh</i>	Heavy hole
<i>lh</i>	Light Hole
<i>e</i>	electron
2DEG	Two-dimensional electron gas
BL	Beer-Lambert-Law
TB	Tight-Binding method
PD	Photo-Detector
QM	Quantum Mechanics
$k \cdot p$	Semiempirical theoretical tool to calculate band-structure
TB	Semiempirical Thight-Binding Method
SOC	Spin-Orbit Coupling, also called Spin-Orbit interaction

LIST OF CODES AND PACKAGES

This list denote the *Open-Source* packages, codes, tools, and repositories to develop this work. All inside of this work as images or numerical calculations are subject to the *Open-Source* ideology. Our codes are it housed in own GitHub repository, both personal as the laboratory repository. It's importantly to say that without develop of Open-Source codes like contents in this list, our codes they couldn't been enhanced.

ASE The Atomic Simulation Environment (ASE) is a set of tools and Python modules for setting up, manipulating, running, visualizing and analyzing atomistic simulations. [5]

SOLCORE A multi-scale, Python-based library for modelling solar cells and semiconductor materials [6]

Aestimo One-dimensional (1D) self-consistent Schrödinger-Poisson solver for semiconductor heterostructures [7]

VESTA 3D visualization program for structural models, volumetric data such as electron/nuclear densities, and crystal morphologies. [8]

PGF/TikZ PGF is a macro package for creating graphics. It is platform- and format-independent and works together with the most important TeXbackend drivers, including pdfTeXand dvips. It comes with a user-friendly syntax layer called TikZ. [9]

SYMBOLS

X⁻ Negative Trion

X⁺ Positive Trion

Al_xGa_{1-x}As AlGaAs semiconductor as a function of Al concentration x

\hbar Planck's constant (eV)

m_0 electron effective mass

(hkl) Family of lattice planes with Miller indices h , k and l

1

PHYSICAL BACKGROUND

In this chapter raise and explains the basis of fundamental physics in semiconductor and quantum structures, implemented to understand the results in this work.

Contents

1.1 Semiconductor Bandstructure	2
1.1.1 Valence and Conduction Bands	3
1.1.2 Excitons	8
1.2 Semiconductor Low-Dimensional Structures	9
1.2.1 Quantum wells	10
1.2.2 Preliminary approach of Quantum Confinement effect in QWs	11
1.3 Summary	14

QUANTUM MECHANICS is basically electron behavior that exhibits many phenomena non explained by classical regime. Quantum structures (QS) are artificially systems conformed by semiconductors where electrons exhibit their quantum nature, this is a great platform to study and create quantum devices. Nowadays, the progress in creation of QS consist in precisely deposition of thin films, in which electrons show fundamentally new electrical and optical properties [10]. Most of these properties consist in quantum behavior as the energy confinement, which is the principal interest to study the electron and their consequent interactions which generates analogous hydrogen atom in semiconductors. Therefore, the interest to studying QS was increasing for many years ago and nowadays, those continue considering an excellent research area.

In this chapter, it presents the fundamental concepts to describe the physical phenomena resultant in this work, without intention to replicate concepts and models already explained in publications with major impact. Therefore, the purpose is to present an own interpretation to highlight the great obtained results.

1.1 Semiconductor Bandstructure

To starting with physical background to understand the QS, it has to start with understand the band structure of semiconductors. The band structure describes the electron behavior in a solid, therefore, we will need to invoke the Schrödinger equation to describe it behavior. But, due inside a solid around 10^{23} valence electrons contribute to the bonding in each cubic centimeter, this results in a many-body complex problem [11], then the general hamiltonian for a solid has the form [12, 13]:

$$H = \frac{1}{2M} \sum_{i=1}^{N_n} \mathbf{P}_j^2 + \frac{1}{2m_0} \sum_{j=1}^{N_e} \mathbf{p}_j^2 + \frac{Z^2}{2} \sum_{i,j=1, i \neq j}^{N_n} V_c(\mathbf{R}_i - \mathbf{R}_j) - Z \sum_{i=1}^{N_n} \sum_{j=1}^{N_e} V_c(\mathbf{r}_j - \mathbf{R}_i) + \frac{1}{2} \sum_{i,j=1, i \neq j}^{N_e} V_c(\mathbf{r}_i - \mathbf{r}_j). \quad (1.1)$$

Where N_n is the number of atomic nuclei, N_e is the number of electrons with mass m_0 , asumming that the nuclei are the same mass it's consider M and charge Z_e . As is obviously, this Hamiltonian is so complicated, the sum of five terms which consists in : kinetic energies to electrons and nuclei, the nucleus-nucleus, nucleus-electron and electron-electron Coulomb interactions, also \mathbf{R}_i are the positions of the nuclei and \mathbf{r}_j are the position of the electrons, the operators \mathbf{P} and \mathbf{p} are momentum operators to nuclei and electrons respectively. Finally, the consider of Coulomb potential V_c [12].

Fortunately, the QS are formed by crystalline materials, the Bloch theorem provide the most important tool to develop required equations. The Bloch theorem establish a periodic potential $U(\mathbf{r})$ for electrons, this due the material is periodic (definition of crystal structure) and the Schrödinger equation it can describe in terms of single electron as:

$$\left[-\frac{\hbar^2}{2m_0} \nabla^2 + U(\mathbf{r}) \right] \psi(r) = E\psi(\mathbf{r}) \quad (1.2)$$

The principal reason that the periodic potential in a crystal structure is highly important is their translational invariance concept and the consequent symmetry operations that are possible in a crystalline solid. The symmetry concept, as a tool to understand solids, is discussed with major detail in the next chapter. In according to Bloch's theorem we can associate a wave vector \mathbf{k} with each energy state, $E_n(\mathbf{k})$. Thus, it is useful to display the energies $E_n(\mathbf{k})$ as a function of the wave vector \mathbf{k} . This result also knowing as dispersion relation, but in general terms is the electron band structure of the given solid [11].

Even if, the calculation of electron band structure in solids are very complex by the distance between atoms that composes it's, and the Bloch's theorem provide the most important tool to reduce the problem to crystalline structures, exists several methods to calculate the realistic bandstructure for semiconductors that are categorized in two groups: Atomistic methods* (Tight-binding, orthogonalized plane wave methods) and Perturbative methods $(\mathbf{k} \cdot \mathbf{p})^\dagger$. These two main categories with theirs respective methods have special characteristics which becomes in the reasons to choose them. The reasons have to do with to the described bandstructure, this mean, in case of Atomistic methods the entire bands (valence and conduction) can describe, but in case of perturbative methods are reserve to near bandedge bandstructures. So, each of these methods can be chosen and enhanced as the system to study requires. We won't enter in discussion about of which of these methods are the best, the reasons are simple, each method is powerful, and we must be remembered that the complexity of solutions requires that these are solved by numerical techniques therefore this convert it to good approximations. Then, basically the electron behavior inside a semiconductor consist in solutions of the appropriate Schrödinger equation [14].

1.1.1 Valence and Conduction Bands

The most important characteristic of semiconductors even we can call as the fingerprint of these, is their bands structure, this characteristic sort out the solids as insulators, metals, and semiconductors. These are the reason of many mechanisms and phenomena

*In this category can include the ab initio methods, these are the most complex methods due to propose solutions of the many-body problem

[†]In fact, both TB and $\mathbf{k} \cdot \mathbf{p}$ also consider in same kind, because both are *semi-empirical* methods due to they consider experimental parameters.

by which study this structures. In general, the bands of semiconductors composed by valence and conduction bands separated by a region known as bandgap. The bandgap, which is proportional to separation energy of valence and conduction bands also is called as forbidden region, this is because doesn't exist electron states, therefore this gap energy determine the electron conduction in a semiconductor and the difference they have with the insulators and metals as shows Figure 1.1.

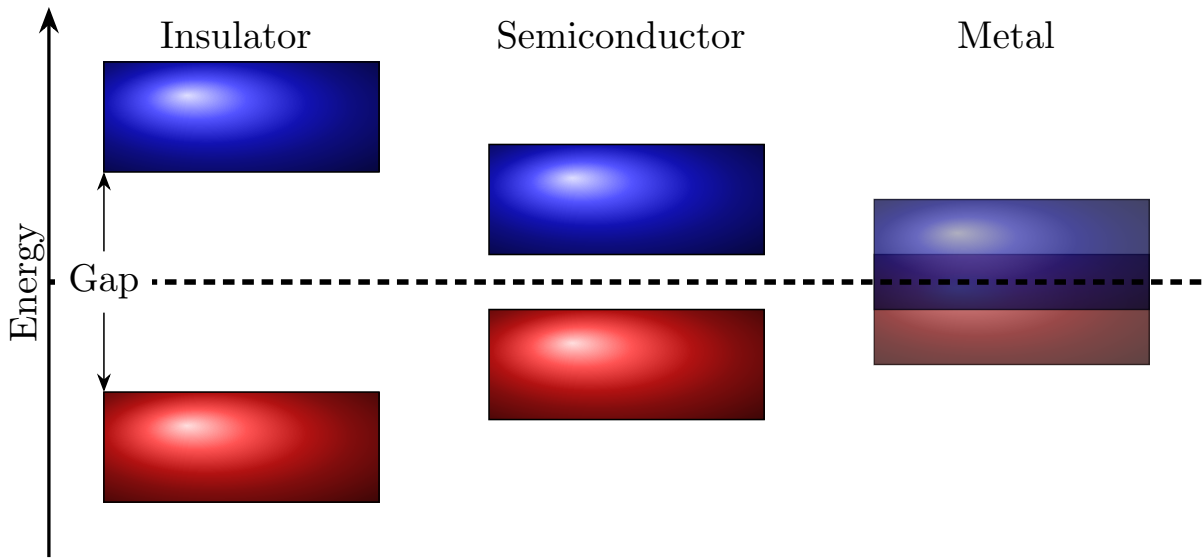


Figure 1.1: Band energy diagram for insulators (left), semiconductors (center) and metals (right). The principal difference is the gap energy, for insulators this is longer than semiconductors, although in semiconductors gap energy depends on materials, finally in metals doesn't exist gap energy instead exist an overlap bands characterize these. Dashed line determine Fermi's level.

So, the bandgap determines many characterizes and functionalities in semiconductors. The bandgap energy classifies semiconductors in direct and indirect semiconductors, but doesn't only depend on this energy, in reality the band structure is the liable for this. As before mentioned, it is so difficult to describe electrons behaviors over the solids due to the many body interactions that exists in its, and therefore the Schrödinger equation that's describe electrons behaviors is complicatedly to solve. Fortunately, the semiconductor structures have one of the most important characterize and his has to do with their atomic structure, that's periodically arrangement of atoms. This periodicity is the key to propose solutions and describe the semiconductor band structure. Starting with describe bulk semiconductors, for example GaAs which consists in with the family III-V cube semiconductor so that their lattice structure consist in a two sublattices correspond to each atom which it conform as shows in Figure 1.2. For this case, when the atoms in two sublattice are different, the crystal structure is then called *zinc-blende* [15].

To calculate bandstructures of bulk semiconductors it's important to define specific symmetry direction, this mean that it's not possible to plot dispersion relation. For each three-dimensional wave vector \mathbf{k} , then the plot energy as a function of \mathbf{k} is along

of different high-symmetry directions [11]. In this work the structures to study are composed of semiconductors III-V, being GaAs the bulk in each structure. GaAs is a direct semiconductor so that the [001] direction is the high-symmetry direction then is denoted by Γ point (at $\mathbf{k} = 0$)

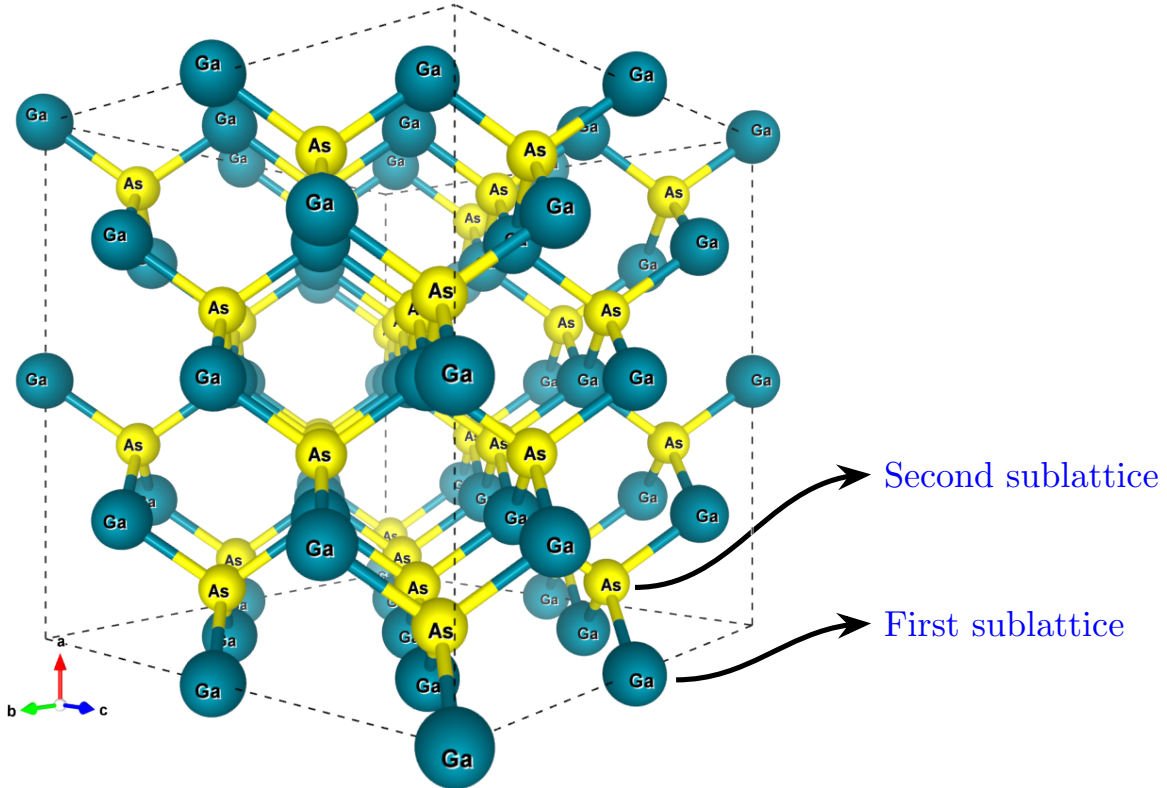


Figure 1.2: GaAs crystal lattice, where the each sublattice correspond of each atom species Ga and As.

As before mentioned several times, it's very complex to compute the Schrödinger equation in the solids. The most “exact” compute is employed by DFT theory, these calculations commonly are called atomistic even some semiempirical models can consider as atomistic, but the semiempirical models are good approximations in comparison with the DFT theory. So, which is the reason to call “exact” solutions to the DFT results? The answer leads us to great discussion and it's not intended to get into controversy, but in general the DFT calculations have the capacity to calculate in terms of electrons interaction and the empirical methods are based in potential choice.

We will, don't into details about band calculations theories and models, but we will make a general reference to the importance in this work. The models more performed in semiconductor heterostructures as GaAs/AlGaAs are semiempirical, this is because DFT theory and their derived models are very limited to carried out in large structures,

their electron interaction nature need high computational perform. So that in comparison with empirical models where the main role is the potential of semiconductor structures, this reduces computational reduce. So, the most models used in semiconductor band calculations are empirical models, these models are distinguished by low computational requires for this reason are considered like approximations. The importance to discuss these concepts will take relevance when we discuss the physics model proposed in this work.

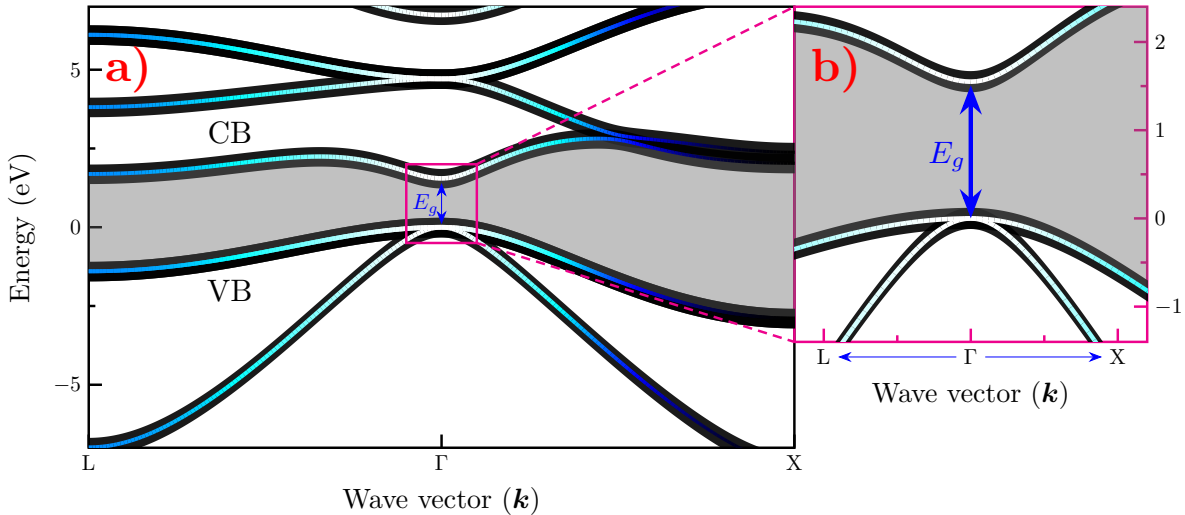


Figure 1.3: Band structure of GaAs, (a) shows the zoom around of Γ to denote the direct band gap and the electrons energy needed to jump from valence to conduction band. (b) denotes the two directions to dispersion of the bands corresponds to Brillouin zone: $\Gamma \rightarrow X$ and $\Gamma \rightarrow L$. [1]

The Section 1.1.1 shows the results of calculations of TB model as discuss it in [16] and the code was implemented by R. Muller [17]. The model purposes by Vogl et al. take into account small number of localized pseudo-orbitals and based the empirical parameters to substitute on TB Hamiltonian. The importance to get bandstructure it's based importance to study optical properties of solid structures, if it doesn't exist band electrons it's like look a place without map, so, the band structure far from being a complex tool it's the key to get the information to investigate the optical properties.

As shown in Figure 1.3(a) the GaAs bandstructure shows that it's a direct semiconductor as a previously mentioned, this gives way to get electron transitions from VB to CB and the energy to success this it. In Figure 1.3(b) it's plotted, the band dispersion around Γ point, it's the most symmetry point. It is well-known that the band dispersion increasing \mathbf{k} along two different directions of the Brillouin zone, from $\mathbf{k} = (0, 0, 0)$ to X point $\mathbf{k} = (2\pi a_L)(1, 0, 0)$ and L point $\mathbf{k} = (2\pi a_L)(1, 1, 1)$. So, these figures, are the typical representation of direct gap to III-V semiconductors around of $\mathbf{k} = 0$, then, is obviously that the shape of dispersion is parabolic. For the GaAs bandstructure calculations shown

in Section 1.1.1 doesn't take into account the contribution of spin*, therefore it's focus on three bands dispersion correspond to a single *s*-like conduction band and two *p*-like valence bands. Is important to say that the characteristic curvature $E-\mathbf{k}$ of dispersion bands corresponds to an electron (*e*) in case of positive curvature while the negative curvature correspond to holes states; heavy (*hh*) and light hole (*lh*) bands, so, this denotes that the transitions, are of dipole nature [1, 13]. All the above disputed is significant to refers of one

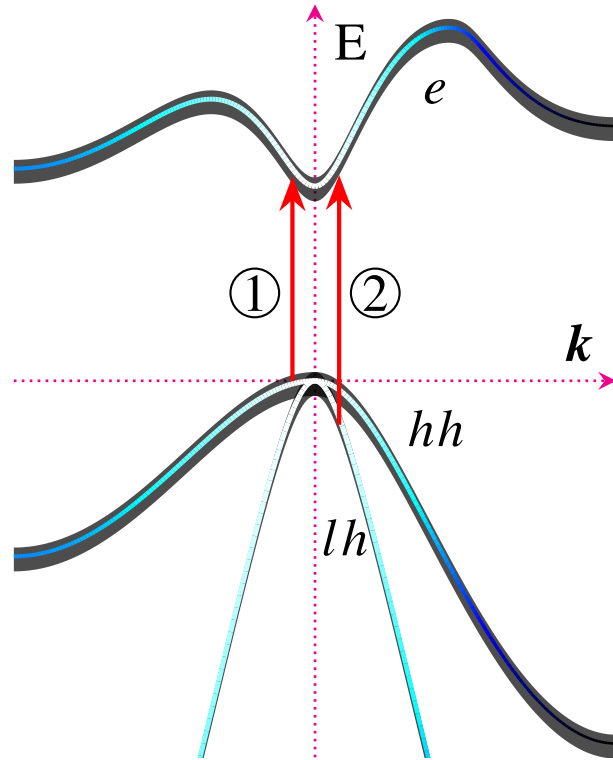


Figure 1.4: Two typical transitions for GaAs near $\mathbf{k} = 0$. The first one correspond to the heavy-hole and second one to the light-hole.

of the most indispensable quantum mechanisms in solids, this is absorption. The electron absorption, specifically interband absorption, give way to a fundamental physical process that involves the principle of many basic studies of semiconductors, applications, and the importance to understand the electron behavior in a semiconductor structures disputed in this work. Then the Figure 1.4 schematizes the two typical transitions in GaAs bulk, this transitions are near to $k=0$, so that is called interband absorption. Is important to remark that the interband transitions are observed in all solids, but the mechanisms are different dependently of their bandstructure, for what, being repetitive when mentioning that the bandstructure is the key to study solids.

In case of GaAs the interband transitions are called as direct transitions, this is because their bandstructure proofs GaAs is a direct Gap semiconductor. This process is determined by quantum mechanical rate $W_{i \rightarrow f}$ for exciting an electron in a initial quantum state

*This spin contribution is called as split-off (so) hole band.

ψ_i to final state ψ_f by absorption of a photon of angular frequency ω [1]. As is very known, this is given by Fermi's golden rule. Later this is disputed according to highlight the model and results obtained. It has been mentioned that the direct transitions are of dipole nature, as before mentioned the CB is type *s*-like while the VB is *p*-like, then it's electric-dipole allowed transitions $p \rightarrow s$. The excitation of electron in CB carries to leave an initial state unoccupied, this is called as a hole creation, then the electron in the final state and the hole is considered as **electron-hole pair**. The next part subject this theme with major focus.

1.1.2 Excitons

The importance to study bandstructure of semiconductors is very clear so far, so that could be said that absorption process is the source of optical properties of solids. It's due to this that the importance to study of semiconductors in the optoelectronics applications. But, this process give rise to formation of one of the most important excitations in the crystal structures. The photon absorption process carries to an electron is excited from CB to VB, this generates an empty location in VB which has positive charge. This positive empty location called as hole, therefore the electron and hole have opposite charge then it's to be expected that they are attracted, so, this creates a bound state called an exciton [18].

From Figure 1.4 and Figure 1.5 is clearly that excitons are commonly presented in direct band gap semiconductors as GaAs, this was denoted by absorption experiments, after mentioned in Section 3.2.1 this is the cause in photoluminescence mechanism.

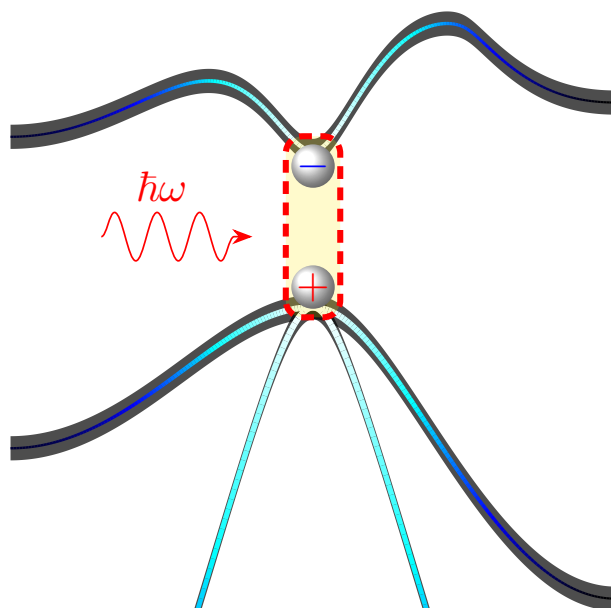


Figure 1.5: Qualitative scheme of exciton creation in GaAs as direct gap.

1.2

Semiconductor Low-Dimensional Structures

The previous section engaged to explain the principles of semiconductors, this is the bandstructure, the importance of these is practically the fingerprint of all semiconductor, without bandstructure the understanding of these would be improbable. The first approximations were based in GaAs bulk, their cubic symmetry practically defines their nature and consequently the physical effects as excitons existence. But, what happens if joined several semiconductors with same symmetry and structural parameters? The bulk properties and physical properties are the same?. The answers they are well-known, when two materials with relatively same structural parameters, as lattice constant can create a heterojunction, the union of several heterojunction make up a heterostructure.*

The Figure 1.6 is a general scheme of a heterostructure, in this case is presents three

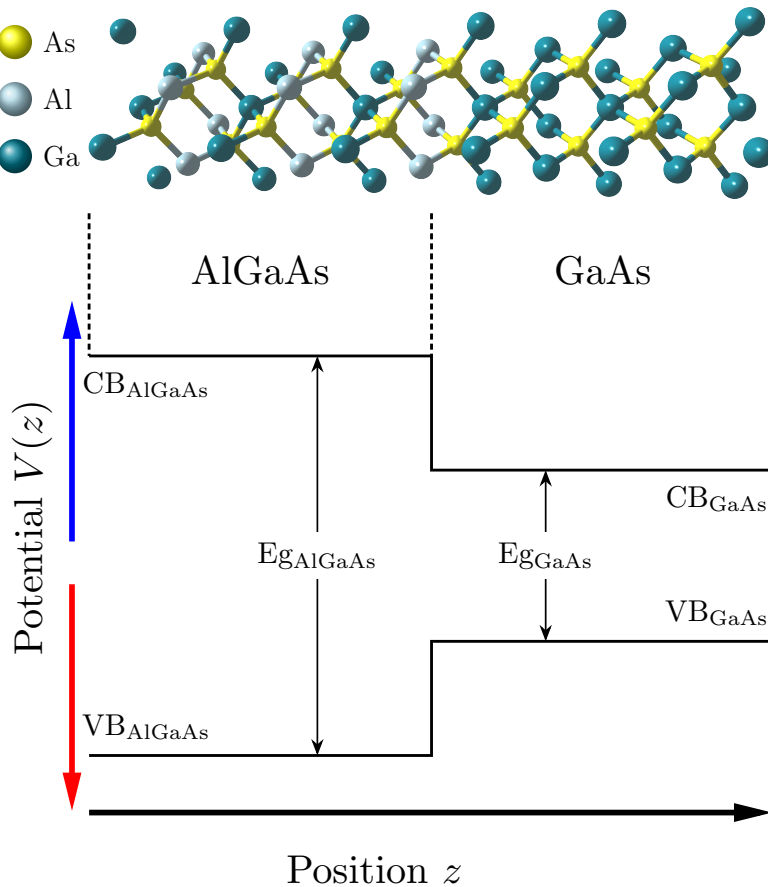


Figure 1.6: General scheme of $\text{GaAs}/\text{Al}_x\text{Ga}_{1-x}\text{As}$ heterostructure, at top show the scheme of atomic arranged of this heterjunction, the dashed lines are the matched between two dissimilar materials. In bottom shows the band-edge profile.

*The samples studied in this work are heterostructures, for this reason, and by nomenclature it's we refer to that way.

species of atoms Al, As, Ga. These atoms can locate in columns III-V of the periodic table, hence its name of III-V semiconductors. The principal characteristic of these atoms is that it can create matched structures as GaAs, AlAs and ternary alloys as $\text{Al}_x\text{Ga}_{1-x}\text{As}$ with specific Al concentration. The matched semiconductors produce a material with new properties based principally in the difference of bandgap which involves the alloys.

As can see in Figure 1.6 it's consisting a GaAs/ $\text{Al}_x\text{Ga}_{1-x}\text{As}$ heterostructure, these interface is well-matched due to the lattice parameters is relatively equals, therefore and thanks to powerful growth technics as MBE it's possible to get high-quality quantum structures.

Also, the heterostructure composed by two semiconductors with different band gaps generate a discontinuity in either the conduction or the valence band can be represented by a constant potential term [19]. The theory to treatment the electron behavior in these structures, is relatively simple if we consider the above. Although, in this chapter doesn't have intention to explore the theory of electron behavior in that, worth noting that it get one-dimensional potential $V(z)$ to both bands, so the Schrödinger equation can solve simple.

1.2.1 Quantum wells

Doubtless the creation or growth of heterostructures increased the interest in the study of quantum structures, the interactions, and physical behavior of light-matter they would not have been possible without these. The major relevance is due the quantum confinement, the junction of semiconductors results in an interest quantum structures with specific dimensions. From 3D bulk the dimensions reduce to 2D, 1D and 0D dimensional structures. Therefore each of that has interest properties and their correspond applications. The Figure 1.7 schematics the low dimensional heterostructures from 3D bulk, the first low dimensional from 3D to 2D is the Quantum Wells, then from 2D to 1D it have the Quantum Wires finally with 0D have the Quantum Dots. The quantum confinement so is the principal reason to study that structures, the electron behavior which exhibits in it should can to help understand a great variety of quantum mechanical phenomena as electron interaction on a crystal. Suppose a heterostructure composed with a two semiconductor alloys as sandwich, this 2D quantum structure is called a Single Quantum Well (SQW).

This dissimilar semiconductors in terms of their potential energy ($V(z)$) can be schematized as Figure 1.8. The Gap difference of $\text{Al}_x\text{Ga}_{1-x}\text{As}$ and GaAs is due to x Al concentration in $\text{Al}_x\text{Ga}_{1-x}\text{As}$ therefore it obtains a one dimensional potential profile, with that can confinement electrons in a 2D plane along z direction. All of these carries to quantum mechanics formalism, the electron behavior should be obeyed these rules. If we have an electron closed in two potential barriers an L distance, the wave which describe it will be spatially confined. So if we confined many electrons in these potential, we have two important physical aspects: the first one is knowing as Pauli's exclusion principle,

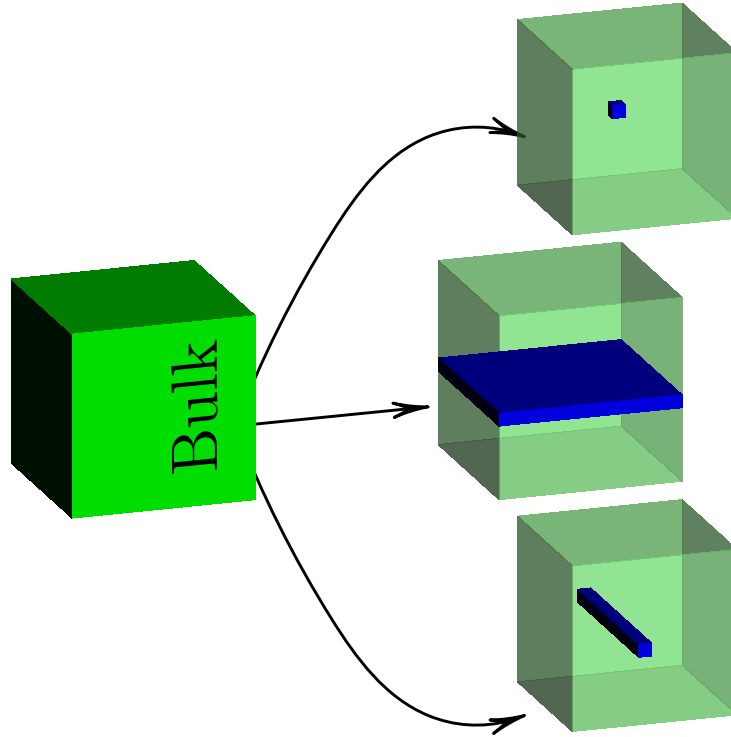


Figure 1.7: Heterostructures from bulk (3D), to Quantum Wells (2D), Quantum Wires (1D) and Quantum Dots (0D).

which as of its Fermion nature prevents carriers with the same spin occupying the same region in of space [19, 20], the second one and one of the most relevant in the birth of the quantum mechanics; the Heisenberg's uncertainty principle. That last, it can say that is the consequence of quantum confinement due to the space reduction of the electrons is expected that momentum increases by an amount of the order \hbar/L . Therefore, the energy of that confined particles increases, and it's referred to as confinement energy [13].

Then the quantum confinement is our started point to understand the optical properties in QWs. As is referred in the figure, the uni-dimensional potential profile can well describe by top conduction- and bottom valence-bands, the band offset in these two of correspond gap energy between that, while Al concentration increases their bandgap and the band offset (Q_c to CB and Q_v to VB) also to.

It's so clearly that the QWs have the potential to presents amazing quantum properties, even if all of these are very important we focus on the optical properties, basically our interest is the light-matter interaction through its result mechanisms.

1.2.2 Preliminary approach of Quantum Confinement effect in QWs

As the title describes, here it will try to explain as the first approach the quantum confinement effect in QWs. If it starts with the scoop, which it can be reduced the

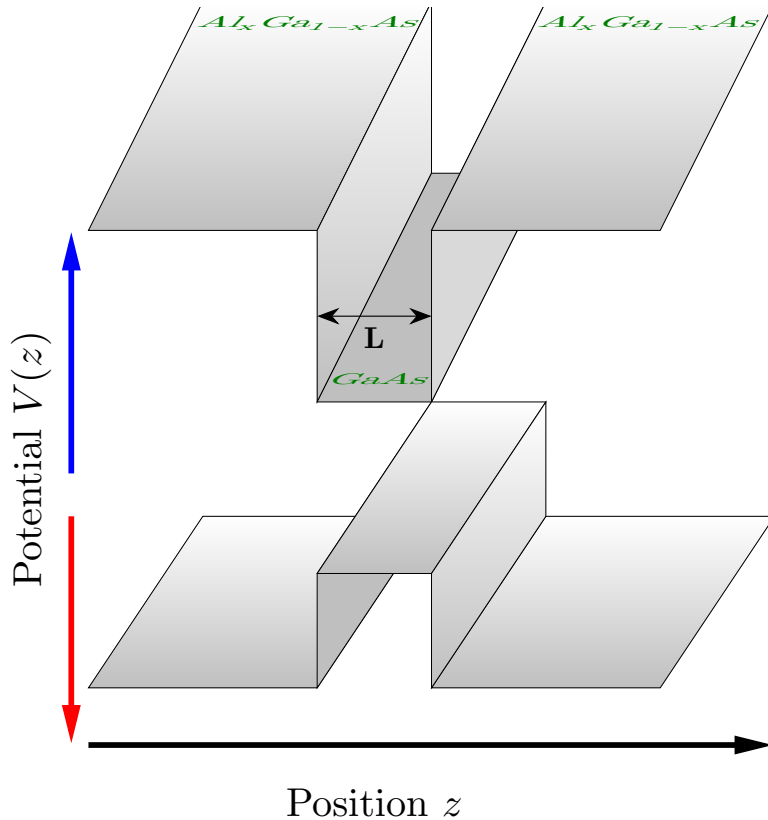


Figure 1.8: GaAs/Al_xGa_{1-x}As Single Quantum Well

electrons space, then this mean that in reciprocal space it has two components k_x and k_y . Then say in crystal symmetry properties to the case of GaAs/Al_xGa_{1-x}As QWs it's Γ the central point, as long as $x < 0.4^*$ the bandstructure depends on confinement energ, so say which the bandstructure depends on confinement energy. In this case, the electronic properties in comparison with a bulk semiconductor properties can solve trough particle-in-a-box as textbook problem as first approach. Nevertheless, even if usually can solver without much mathematical formalism is very essential that it dedicates a chapter with their solution, this is because will employ a physical formalism exclusively to QWs structures. In general way, as it before mentioned the Schrödinger equation solution is the fundamental pillar to understand, where it's taken into account which in a crystal the periodic potential is the key. Here are important remarks before to continue, when it has a heterostructure starting with the bulk model it's clearly that the system doesn't same, the Quantum Mechanics which is behind take into account the symmetry properties, then it can be developed a Hamiltonian to understand that system. In the next chapter will be explained details and the formalism both physical and mathematical to solve and discuss it's. The model which give the tools to get the solutions is called as Effective Mass

*It will be explained in the next section, although it's due to the Gap go from direct to indirect, shortly the symmetry $\Gamma \rightarrow X$.

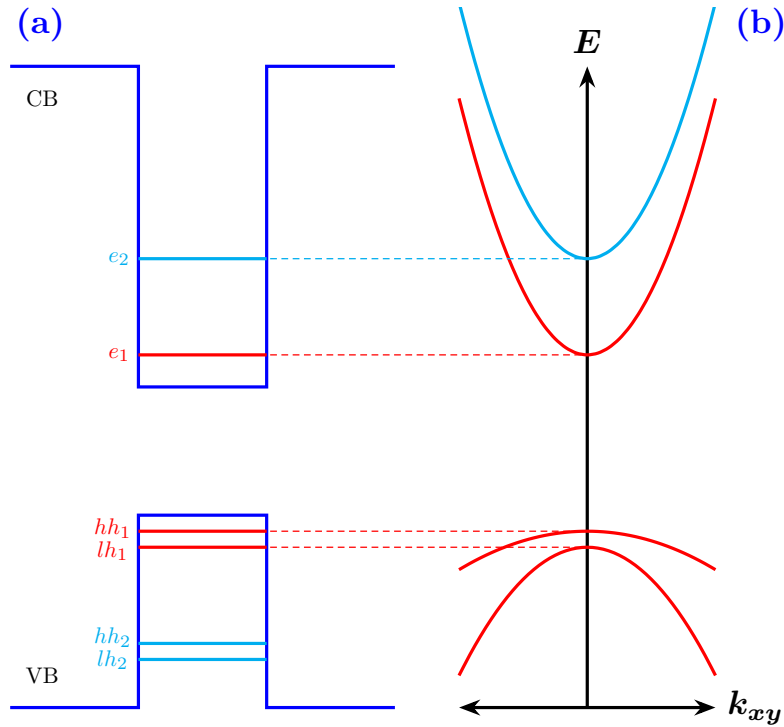


Figure 1.9: General scheme of typical Schrödinger's equation solutions to one-dimensional potential as (a) where the Eigenenergies of both electron and holes are denoted with same color depending on n value.(b) It's plot, of the subbands in the same case of (a) to both particles.

Approximation, thus their correspond Schrödinger equation is [1, 19, 21–24]:

$$-\frac{\hbar^2}{2m^*} \frac{\partial^2}{\partial z^2} \psi(z) + V(z)\psi(z) = E\psi(z), \quad (1.3)$$

where the m^* is the effective mass in each material, and $V(z)$ is the potential profile got by heterostructure materials properties. Therefore, that differential equation can solve as in textbooks explained [1, 19, 21, 23, 25–28]. The idea is thinking as a one particle in a finite potential well, where is well important established the boundary conditions and solve the Schrödinger equation in each part of single QW, this means that need to create a potential function. Then it's can obtain the Eigenfunctions and their correspond Eigenenergies.

The principal idea doesn't is reproducing something which is very well known, the objective of this part is established the scoop of the next chapter. Therefore, before to continue, we will finish with to explain the dispersion in-plane of single QW. As in the QW the one-dimensional potential set up the 1D confinement, is important doesn't confuse which the QW is a 2D structure, but their confinement is along of z direction this mean 1D. Then, the particle can motion in the $x - y$ plane. By this reason, even if consider 3D Schrödinger equation and the above is considered it obtain Equation (1.3) therefore, the solutions in the one-dimensional potential produce discrete states of energy $E_z = E_n$ [19],

where n is the energy level it which produce subbands as shows in Figure 1.9. In contrast, before it called as “energy bands” in the bulk case, now due to the quantum confinement gets subbands to both conduction- and valence bands.

These subbands are the result of the sum of E_z and $E_{x,y}$, which are the 1D confinement energy and the in-plane momentum $k_{x,y}$ then [19]:

$$E = E_n + \frac{\hbar^2 |\mathbf{k}_{x,y}|^2}{2m^*}. \quad (1.4)$$

From equation the effective mass m^* depends on particle, i.e the effective mass to electrons in CB and the holes in VB. So, the most relevant in the solutions is the energy E_n (Figure 1.9(a)) is discrete, this is the quantum confinement in the low-dimensional heterostructures.

1.3 Summary

In this chapter, was exposed the generalities of semiconductor band structure and low-dimensional heterostructures, highlighting or taking in major GaAs/Al_xGa_{1-x}As that's the semiconductors of major importance in this work. The band structure interpretation usually be so hard, and their calculations even more, but the impact and relevance in optical properties of semiconductors starts from that interpretation, from here arises the mathematical arsenal to right physical interpretation. Another significant concept which was treatment as first approach is the effective mass concept, even if, when solved, the bulk Hamiltonian it considers the mass as constant parameter or depending on semiconductor material, contrary in low-dimensional structures have an important role.

In generally, the band structure of semiconductors is the key to understand quantum properties of solids, in this work the relevant is the light-matter. Remember that light-matter interaction in solids can be studied by process resulting in it, as absorption, reflection, transmission, diffraction, scattering, and others [29]. Although, the light-matter interactions are fundamentally quantum electrodynamical, also, can be studied in quantum way through before mentioned process. Firstly, is the photon absorption process can help to understand or calculate the fundamental parameter in semiconductors as is bandgap energy. This parameter is the started point in the study of semiconductors, this is the start point in the map called bandstructure, if it ignores the gap value in the semiconductor to study it couldn't possibly get the principal optical properties of that.

Then, the bandstructure of semiconductors is the map to understand them, without these routes or fundamental parameters couldn't have quantum devices.



PHYSICAL MODEL

In this chapter, it's exposing the fundamental physics to understand the experimental results' through physical model, both numerical and phenomenological. It is emphasis in symmetry properties of semiconductors, which is the base to get our model.

Contents

2.1	The Symmetry Context	16
2.1.1	The symmetry and the Band Structure	19
2.2	Symmetry breaking in Semiconductor Structures	21
2.3	General revision of numerical methods	22
2.3.1	Finite Difference Method	22
2.4	Structural Parameters	22
2.5	Anisotropy model in CQWs	22

SEMICONDUCTORS are alloy of materials with pure structural characteristics, it's the alloys which can generate an amazing quantum process that is quantum confinement. But, all of them couldn't possibly be achieved without understand of semiconductor bands, are bands the reason to get semiconductor heterostructures. Now, the objective is proposing the model to study Coupled Quantum Wells. The CQWs are heterostructures grown from a semiconductor substrate as GaAs as previously treated SQW (see Figure 1.8) but coupled by a thin barrier which have a very significant role. But before to mention the objective of study this structures and the physical model which explain their experimental results is important to call about of the symmetry and their relevance to understand the physics of these QS.

Previously, we were very repeating in the importance of semiconductor band structure, also to remark difficult of get them. It was saying the complexity of calculate semiconductor bands is high, by this reason it's developed models to approximate it. But, all of these couldn't be possible if it would not be taken into account the *symmetry* role in physics [30]. Thanks to symmetry, it's possible to understand from Quantum to Universe. It is clear that to talk the symmetry is inevitable to think in geometry or nature patterns inherently way, but in the next sections it's established the symmetry role from the band structure calculation to the importance in the electron behavior in CQWs structures.

2.1

The Symmetry Context

Talk about *symmetry* is talk of shapes or in a romanticism way as the natural harmony that makes something appear beautiful to us [31, 32]. But, what is the reason the *symmetry* is very important in physics?. The reason the *symmetry* is very important has to do with a *transformation*, this mean that if a physical system is affected or perturbed by a thing and this appears to be exactly the same before and after that *transformation*, it is said to be *invariant* under that *transformation*. The symmetry of the system is made up of all the transformation operations that leave the system invariant [31].

In this section doesn't have the purpose to be a one more copy or re-interpreted version of a group theory book, yes, the group theory not symmetry theory, it's important to remember that to understand of symmetry physics of solids it's important to understand the group concept. In generally, a group is a set or collection of elements that obey certain criteria and are related to each other through a specific rule of interaction and obey four group axioms [31, 33, 34]. It is important to remark which the heterostructure to will study is composed by $\text{GaAs}/\text{Al}_x\text{Ga}_{1-x}\text{As}$ semiconductors, then we started with the GaAs crystal to propound the symmetry role in the CQWs. Then, already raised the starting point, remember that the crystal solid can be defined as an arrangement of atoms in strictly periodic arrays [35, 36], from here arises two concepts: basis and lattice, where that

last is the set of mathematical points to which the basis is attached [35]. These crystal concepts give place of crystal primitive cell in three dimensions also considered as the seed to reproduce a crystal. So, it gets fundamental types of lattices defined by a collection of *symmetry* operations (rotation, translation etc.), then it's compose a lattice point group. In the three-dimensional case, the point symmetry groups require the 14 different lattices types*, where are classified into seven systems. Into these systems it's found the *cubic* system, it which posses three number of lattices. Remember that the GaAs crystal is *cubic*, specifically, is the type FCC lattice. The FCC lattice is easy to imagine, if place an atom in each corner of a cube and in a center of each face of it. Therefore, it is easier to define the planes and crystal directions if we take the cube faces as a reference it gets (hkl) plane and the directions [hkl] which must be perpendicular to a plane (hkl) [35].

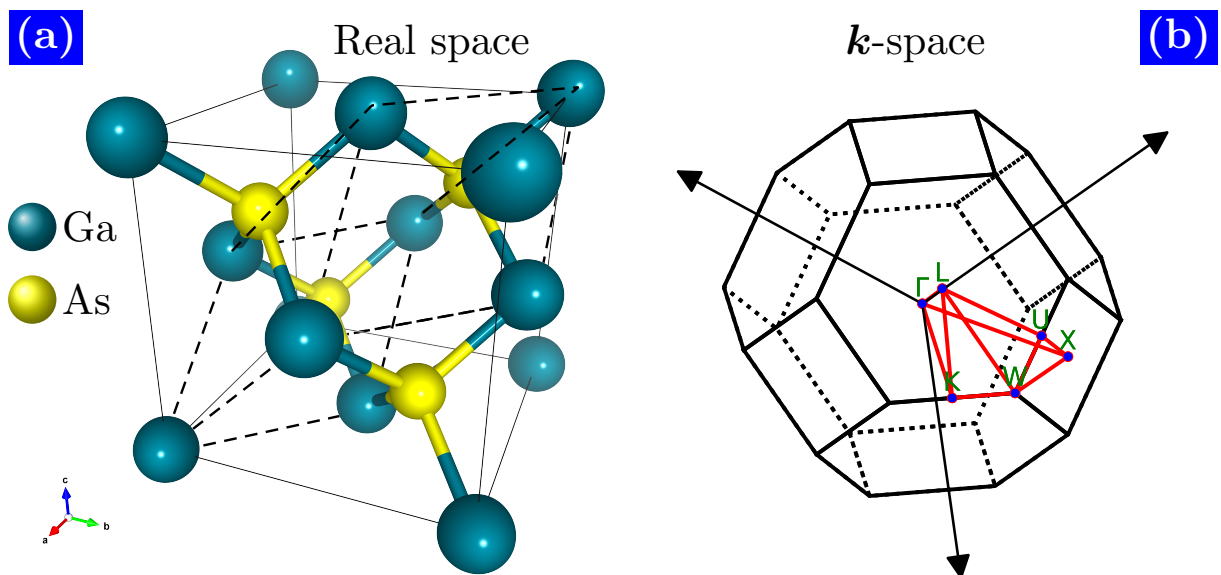


Figure 2.1: (a) GaAs crystal structure in “real space”, this region is known as *unit cell*, into that with dashed line is denoted the primitive cell. This lattice is well-defined by the vectors \mathbf{a} , \mathbf{b} and \mathbf{c} , these vectors are defined as the basis vectors. In (b) is schematized the GaAs crystal structure in k -space, also known as *reciprocal space*.

The lattice is an array of points which make the space lattice of a *crystal* and the repetitions or disposition of these points is controlled by “*symmetry* operations” [37]. The crystal is composed by a space lattice this is a plane lattice[†] which have three *symmetry* operations: *Rotation axes*, *Mirror plane* and *Centre of Symmetry*. If add a one dimension to plane lattice it gets a space lattice, which define the unit cell of a *crystal*, so this adds one more *symmetry* operation which is *Rotation Inversion* or *Roto-Inversion*. Then, can get *symmetry* elements of a *crystal* if apply the four *symmetry* operations and their possible combinations. If collect that *symmetry* elements obtains the *point symmetry* or the *point*

*This lattices are known as Bravais Lattices

[†]2D point pattern array

group of symmetry of a *crystal*. The GaAs crystal as before mentioned is a *cubic* system, but have a defined *cubic* structure called as *cubic zinc sulfide* or simply *zincblende*. This specific *cubic* structure is characterized by arrangement of two type atoms with places coordinates: $000, 0\frac{1}{2}\frac{1}{2}, \frac{1}{2}0\frac{1}{2}, \frac{1}{2}\frac{1}{2}0$ for one type of these as Zn in ZnS or Ga in GaAs structure. In case of the second one atom, it has coordinates : $\frac{1}{4}, \frac{1}{4}, \frac{1}{4}, \frac{1}{4}, \frac{3}{4}, \frac{3}{4}, \frac{3}{4}, \frac{1}{4}, \frac{3}{4}, \frac{3}{4}, \frac{1}{4}$ for S in ZnS or As in GaAs [35, 38]. The Figure 2.1(a) shows the unit cell of GaAs structure and into them it dashed the primitive cell for the FCC lattice, also denoted the basis vectors \mathbf{a} , \mathbf{b} and \mathbf{c} .

In the case of symmetry of GaAs crystal, is important to remark that this symmetry can also denote in Hermann-Maguin notation $F\bar{4}3m$ which corresponds to three fourfold rotary inversion parallel to the edges of a cube, with four threefold rotation axes parallel to the body diagonal and six mirror planes, each containing a face diagonal [37]. The F label corresponds to cubic system FCC, following by the corresponds operations.

The symmetry context before exposed can view as a macroscopic symmetry about a crystal system, which means, is very interactive to think as a pattern well-ordered can conform a plane lattice and is intuitively work the symmetry operations. But it's not the only symmetry concept in crystal systems, if we enter into crystal it found atoms or molecules which conforms it. So, the internal study of a crystal add two symmetries to the actual worked before. These "microscopic symmetry" [37] the make reference to \mathbf{k} -space or reciprocal space. So, the previous concept of lattice it's also known as direct space lattice. Thanks to X-Ray, Electron or Neutron diffraction techniques, it was possible to study the internal structure o crystal symmetries in the reciprocal space, this trough diffraction phenomena, the propagation of waves into crystal can to form well defined pattern they which are explained by the wave-vector concept [31, 39]. Therefore, is expected that the electron wave function can be denoted with a lattice periodic part $u(\mathbf{r})$ and wavelike part $e^{i\mathbf{k}\cdot\mathbf{r}}$ so, the set of all wave vectors \mathbf{k} corresponds to plane waves due the lattice, this is known as reciprocal lattice [40]. Then taken into account this, and the vectors \mathbf{a} , \mathbf{b} and \mathbf{c} in reciprocal space can describe the total unit cell [31, 40].

Finally, as a result to get the unit cell in reciprocal space and known which this is composed by lattices, these lattices are called as *Brillouin zones*. Practically the *Brillouin zones* are constructed by drawing the vectors \mathbf{K} defining the reciprocal lattice and then bisecting each of these with planes perpendicular to \mathbf{K} [31]*. In Figure 2.1(b) it's schematized the *Brillouin zone* to GaAs crystal structure, specifically this representation is called as *first Brillouin zone*. To GaAs crystal it was defined the symmetry operations which compose the symmetry elements in Hermann-Maguin notation as the point group $F\bar{4}3m$, it's important to consider the Schoenflies notation also, this due people often speak in terms of both, although the Hermann-Maguin notation is consider as the International notation. In Schoenflies notation, the GaAs correspond to T_d point group.

*The wave vector \mathbf{K} is defined in [41] equation (1.5)

2.1.1 The symmetry and the Band Structure

Returning to Figure 2.1(b), the Brillouin zone have labels which they are, importantly, this is because each of these denote a point group symmetry. These points are: Gamma, X, L, W, U, K. In Schoenflies notation these correspond to: $\Gamma \rightarrow O_h$, $X \rightarrow C_{4v}$, $L \rightarrow D_{3d}$, $W \rightarrow C_{4v}$, $U \rightarrow C_{2v}$, being Γ the high symmetry point. Then, why is the importance of the **BZ** role in semiconductor band structure?, the answer is the aim of this subsection. We started with the first section of this work, in it refer the importance of solution of Schrödinger equation, specifically at crystal structures as semiconductors. Here, the most important tool is the Bloch's theorem, it which is developed from periodic property of crystal so, it's possible to approximate.

This context is introductory and general, because this doesn't possible if not consider the symmetry properties in crystals, in fact, *the symmetry of system define the basis function to get the electron band structure* [13, 42–44]. Remember that the concept of *basis function* is a mathematical concept, which in quantum mechanics it's known as *Wave functions*. Also, never to forget which the *symmetry* concept is inherent in physics. Therefore, the Group theory establishes the game rules. So, the **BZ** is the result of Group theory applied in crystal structures, then the **BZ** is the map to understand the electron behavior in crystal structures, this defined the \mathbf{k} points trough high symmetry paths, where this starts at Γ point or $\mathbf{k} = 0$. If observe the Section 1.1.1 the horizontal axis correspond to \mathbf{k} points and labeled the high-symmetry directions from Γ , then this is the \mathbf{k} paths in **BZ** as can see in Figure 2.1(b).

Previously, it's continuously mentioned which band structure calculations are difficult, so, it will start to change the hard word to tricky, this because it's possible to make very good models and approximations taking into account the symmetry of the system. All to begins from symmetry, the well-known models to calculate band structure starts from symmetry arguments of crystal or the semiconductor studied, through succession of symmetry operations it knows until it's invariant, this mean doesn't change under transformation. Here, highlights the invariants concept, which is the connection of symmetry and Quantum Mechanics. The symmetry gets the information of the system, while the QM the information of the state electrons. The Hamiltonian of the crystal has a symmetry which depends on their potential, then the crystal potential posses a point group, which is invariant under any transformation. So, the solution of the Schrödinger equation contains the state of the system. From these tools, can propound the physics of electrons or another quasi-particle inside a semiconductor, for example in perturbation theory, starts from Hamiltonian \mathcal{H}_0 with it specific space group, but under perturbation the Hamiltonian of the system should be the sum of $\mathcal{H} = \mathcal{H}_0 + \mathcal{H}'$, where this last has the symmetry correspond to a subgroup of the \mathcal{H}_0 group. This is, the principle of this work which after will be discussed with detail. While the solution of Schrödinger equation with the total Hamiltonian \mathcal{H} will result in the energy spectrum $E(\mathbf{k})$ along of the **BZ**.

Being a crystal system and the potential is the periodic, it's to hope which a multiband spectrum. Although here doesn't consider the degeneracy* term, it's evident which the Group Theory has the solution, in general words, are the irreducible representations of the symmetry group which determine the dimension of degeneracy [45].

Thus the band structure as a whole exhibits the symmetry characterized by the crystal [45]. All previous it's about of an ideal crystal, then it's possible to get exact solutions of Schrödinger equation. But, to determine in detail the spectrum $E(\mathbf{k})$ throughout the **BZ**, one needs a numerical solution of the Schrödinger equation. In previous sections, it shows the results of apply **TB** method to GaAs bulk, this method parts from Bond Orbital Model [16, 46, 47], in this case, the basis functions it's forming linear combinations of atomic orbitals (LCAO) to specific symmetry group [42].

In this method, the importance is the arrangement of atoms and their orbitals considered, for Figure 1.2 these are sp^3 . In another way, in the case of $\mathbf{k} \cdot \mathbf{p}$ method, apart from perturbed model, but in both the main idea it's found the \mathbf{k} -points correspond to the symmetry of the system. In another way, in the case of $\mathbf{k} \cdot \mathbf{p}$ method, apart from disturbance model, but in both the main idea it's found the \mathbf{k} -points correspond to the symmetry of the system. The difference apart from their basis is the efficiency in their applied over semiconductor structures, this means that the $\mathbf{k} \cdot \mathbf{p}$ -method is appropriate in a small region of **BZ** to describe $E(\mathbf{k})$, therefor is the preferred option to describe semiconductor bands around of Γ , while if the idea is describing $E(\mathbf{k})$ in an extended region of the **BZ** the **TB**-method is the correct [42, 45]. In any way, the symmetry establishes the basis to get semiconductor band structure, no matter the method this, includes the first principle methods as DFT, which requires the symmetry information of the system to get the pseudopotentials and the geometric optimization to enhance calculations.

Although the symmetry concept is the base, the principal objective in this work you have to see the consequences of symmetry under in a non-direct perturbation, this mean, if it has GaAs bulk-semiconductor this has one defined point group T_d . When applied it a perturbation, as an electromagnetic perturbation the principal symmetry group it's reducing to a subgroup of itself. This is to mean which the subgroup is also invariant. This conception is also knew or called *symmetry breaking*. It this concept, it was employed at first time by Pierre Curie at ended of nineteenth century [48], It this concept, it was employed at first time by Pierre Curie at ended of nineteenth century, he establishes that, if happens thing which doesn't allow system invariance, so the original symmetry it's lowered then, this mean which symmetry is broken. But, what is the importance to focussing on that ?. The importance of symmetry breaking is the physical effects that are presents, the properties of semiconductors changes under reduce symmetry and this can observe in band structure. In the next section will be discussed the importance of symmetry breaking in semiconductors and above all over QWs.

*This is due to the linear independent solutions, which corresponds to one energy, this mean m -fold band degeneracy at the point \mathbf{k} [45]

2.2Symmetry breaking in Semiconductor Structures

The symmetry breaking, it's the basis for the physical model in this work. Starting off from the general and brief concept of the symmetry importance in the Solid State viewed in the past section, it will arise the symmetry role and the reduce symmetry in CQWs. Before to start the history, is important to clear that

2.3General revision of numerical methods

Some physical systems can be explained through models that can solved analytically assume nearby experimental parameters but in realistic cases analytical models doesn't enough to obtain approximation of the experimental results. In past computational time and technology limitations they did not allow solving numerically large system of equations. Nowadays, numerical solutions do not represent a problem because computational systems allows solving large system of equations in a few time. In this work was implemented a numerical solution of one-dimensional Scrödinger using finite-difference method the principal reason to use this is that, basically represent the solution of an eigen-value problem.

The solution of typical problem in quantum mechanics is the single well with infinite barriers, this is a one electron trapping inside a well like a see in the next figure

The electron has zero potential energy in the region $0 < x < a$ where a is the width of well, how previously comment the Scrödinger equation

2.3.1 Finite Difference Method

S

2.4Structural Parameters

2.5Anisotropy model in CQWs

3

EXPERIMENTAL DETAILS AND RESULTS

In this chapter shows the experimental result of each sample employed. The chapter is organized by sample name.

Contents

3.1 Samples Description	24
3.2 Spectroscopy: Experimental setups and experimental results	27
3.2.1 Photoluminescence Spectroscopy (PL)	28
3.2.2 Photoreflectance spectroscopy (PR)	36
3.2.2.1 Excitonic effects	42
3.2.2.2 The PR summary	51
3.2.3 Reflectance Anisotropy Spectroscopy (RAS)	51

3.1 Samples Description

QUANTUM STRUCTURES were created thanks to the technic Molecular Beam Epitaxy (MBE) growth which in general terms consist in great precision of the growing thin films of semiconductor materials, through high precision deposition on a suitable crystalline substrate. As has been pointed out on many occasions, MBE is nothing more than a sophisticated form of vacuum evaporation* [49], this does not sound bad but the MBE technique is not only this, epitaxial growth needed the precision in experimental growth parameters how temperature, deposition rate calculations, REED analysis, etc. So that in a bit of words the purpose is to supply appropriate atoms or molecules to the substrate surface and leave surface diffusion, surface reactions and inevitable desorption from the surface to play their various roles in generating an epitaxial film [49, 50].

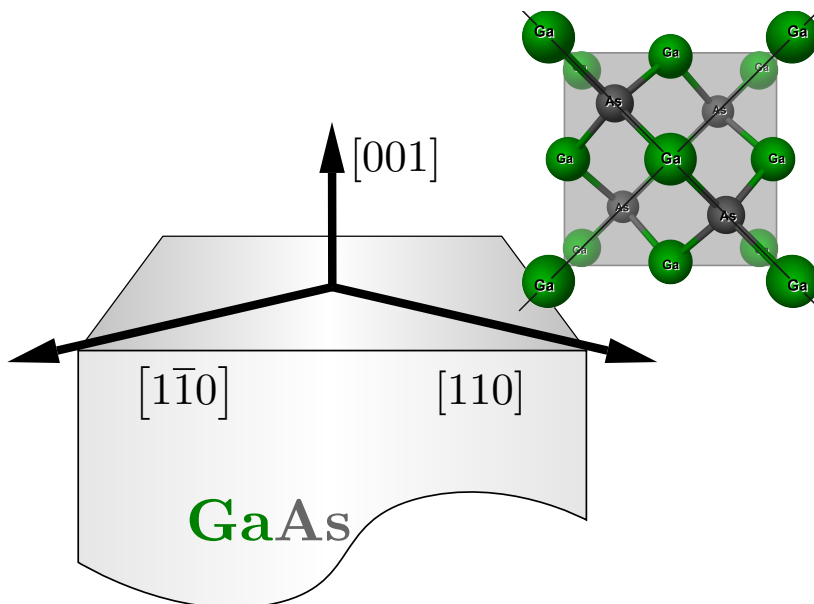


Figure 3.1: GaAs substrate

The samples studied in this work, are made up of a GaAs (001) substrate, the GaAs substrate has a zincblende-type crystal structure, in which the atoms are tetrahedrally coordinated Figure 3.1 the choice of crystal is very important and preparation of these can modify the growth result, for this reason, the high quality of substrate is the basis of growth of heterostructures. The heterostructures are a combination of more than one semiconductor, this leads to the superlattice definition where more of two semiconductors are

*In owner experience, MBE growth is a very exhausting task, so great respect to all people that works on this

atomically deposited over the substrate in the growth direction (001). The semiconductors used in the samples are GaAs and AlAs then these can have different thicknesses, growing periodicashowgrid][lly and alternately way over the substrate with thickness $d_{\text{GaAs}} + d_{\text{AlAs}}$. The result consists in an arrangement of $(\text{GaAs})_2(\text{AlAs})_2$ superlattice, like a shown in Figure 3.2 or AB arrangement like a said commonly. In QWs structures, the width is the principal characteristic because quantum confinement is dependent on this, then MBE is the perfect choice to realize this.

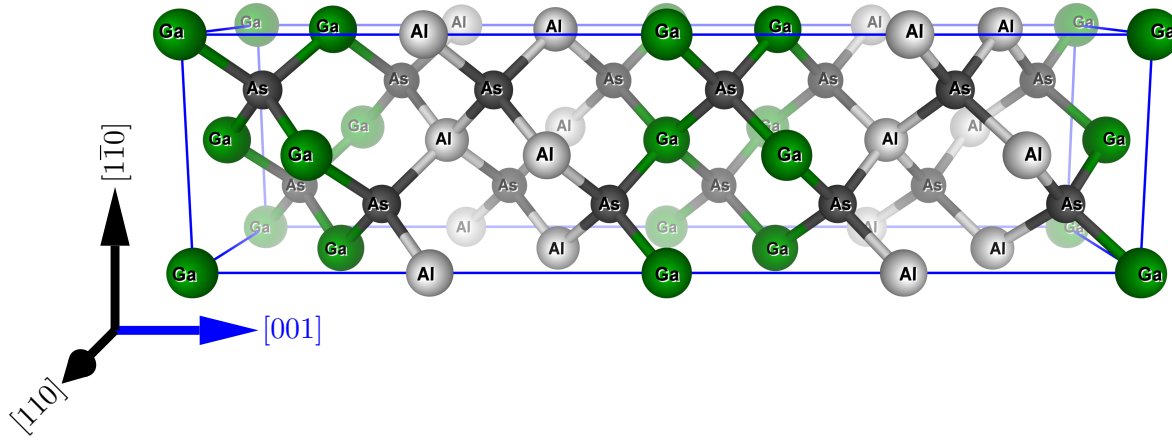


Figure 3.2: Atomic order in AlGaAs crystal structure grown along (001) direction.

The realistic structures present some details that can modify the experimental results, some of these are inevitability due to the complexity of growth. One of these is the interfaces between two different materials, i.e., the typical structure of GaAs/AlGaAs has an interface between these, then the problem is due to an imperfect mismatch of materials, therefore, can cause anisotropy effects. Other details which usually are considered are surface, point defects along of structure, or strained caused by overlayer in the epitaxial process. Later, the interfacial detail gives the physical sense to RAS experiments in the symmetric CQWs structures.

Table 3.1 shows the sample names, each sample has two QWs coupled by a thin barrier preferentially of $\text{Al}_x\text{Ga}_{1-x}\text{As}$ semiconductor where Al percent is important because of the barriers potentials depends on this, in the case of AlAs barriers the potential barrier is bigger than $\text{Al}_x\text{Ga}_{1-x}\text{As}$. As a before-mentioned, this was taken into account in numerical calculations to generate the potential profile. Commonly for the case, $\text{Al}_x\text{Ga}_{1-x}\text{As}$ barriers both in adjacent like the coupling barrier the x values are in the interval $0.1 < x < 0.4$. Worth mentioning that the purpose of the first four samples (up to down in table) they were grown with the objective of measure indirect excitons (IX), so that, the structures are more complex, and we omitted the value of n-doped since these samples are doping in bottom and top to minimize the intrinsic electric field (screening field effect) so that external perturbation is applied through a voltage over the sample [51] and the n-doped

enhance the external perturbation *. After realized experiments over the four first samples and observe possible trions (\mathbf{X}^+ or \mathbf{X}^-) through PR spectroscopy and an apparent increase of the RAS signal, it was decided to focus the experiments on these structures, which have a less complex composition as in the case of the first three samples in the table (see Table 3.1). Therefore, it took the sample M4_3141 as a basis, i.e., same barriers widths both coupling barrier and adjacent barriers, obtained the samples M4_3521 , M4_3522 and M4_3523 where sample M4_3522 is the same to sample M4_3521 in structure but with a different type of doping (p-type in M4_3522 and n-type in M4_3521), samples M4_3521 and M4_3522 have the same doping type (n-type in both) but one of the QW is more width to another, this means that the sample M4_3523 have the same thickness in both QWs (SCQWs) and sample M4_3521 have one QW thick more than the another (ACQWs).

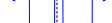
Sample name	NW width (nm)	$V(z)$	WW width (nm)	Barrier width (nm)	Barrier	Adjacent barriers	Doped type	$\left[\frac{1}{cm^3} \right]$
M4_3171	11.87		13.85	3.960	AlGaAs	Al _{0.15} Ga _{0.85} As	n[Si]-i-n[Si]	6×10^{18}
M4_3172	11.87		13.85	0.565	AlAs	Al _{0.30} Ga _{0.70} As	n[Si]-i-n[Si]	6×10^{18}
M4_3226	11.87		13.85	0.424	AlAs	Al _{0.30} Ga _{0.70} As	n[Si]-i-n[Si]	6×10^{18}
M4_3140 (ACQWs-1)	11.87		13.85	1.980	AlGaAs	Al _{0.15} Ga _{0.85} As	i-n[Si]	6×10^{18}
M4_3141	11.87		13.85	3.960	AlGaAs	Al _{0.15} Ga _{0.85} As	i-n[Si]	6×10^{18}
M4_3521 (ACQWs-2)	11.87		23.74	1.980	AlGaAs	Al _{0.15} Ga _{0.85} As	i-n[Si]	6×10^{18}
M4_3522 (ACQWs-3)	11.87		23.74	1.980	AlGaAs	Al _{0.15} Ga _{0.85} As	i-p[Be]	5×10^{16}
M4_3523 (SCQWs)	11.87		11.87	1.980	AlGaAs	Al _{0.15} Ga _{0.85} As	i-n[Si]	6×10^{18}

Table 3.1: This table shows the CQWs structures studied in this work. CQWs potential profiles $V(z)$ are shown to observe the different shapes, composition parameters, and dimensions of structures studied. The dashed line determines the symmetric reference in the last samples in which we focused (M4_3141 , M4_3521 , M4_3522 , M4_3523), due to their characteristic results.

The Section 3.2 shows each experimental setup implemented in this investigation with their respective results. Starting with the Section 3.2.1 shows PL spectroscopy, their experimental setup implemented to obtain transitions energies values and compare with numerical results, after, in Section 3.2.2 shown experimental setup and results of the PR spectroscopy, to get information about the intrinsic electric field and the effects caused by this. Finally, Section 3.2.3 shows the RAS experimental setup and exposes the experiments that were realized to study the anisotropy caused by the asymmetry due to the relative thickness between the CQWs.

*Non-published, the specific information about the doped in these growths, if you have a question about this, you can send email to Dr. Klaus Biermann biermann@pdi-berlin.de

3.2

Spectroscopy: Experimental setups and experimental results

OPTICAL SPECTROSCOPY frequently is defined as a branch of physics that studies the *light-matter interaction*, this is important because the simple definition of interaction covers a vast realm of physical phenomena from classical to quantum electrodynamics [52]. Therefore, optical spectroscopy is an essential tool in experimental solid state physics, gives the guide to study optical and electronic properties of semiconductors.

The optical process in semiconductors consists of the study of response due to *light-matter interaction*, this response corresponds basically to the processes that can occur in the solids when light* falls on (photons) in it. These processes are absorption, reflectance, emission, and scatter where all of this depends on electromagnetic spectra range, in our case this range includes from near-infrared to mid-infrared (700nm to 900nm). Although those processes are of the utmost importance, optical spectroscopies that uses in this work involve more interest in absorption and emission, being the latter sensed in our experimental setups.

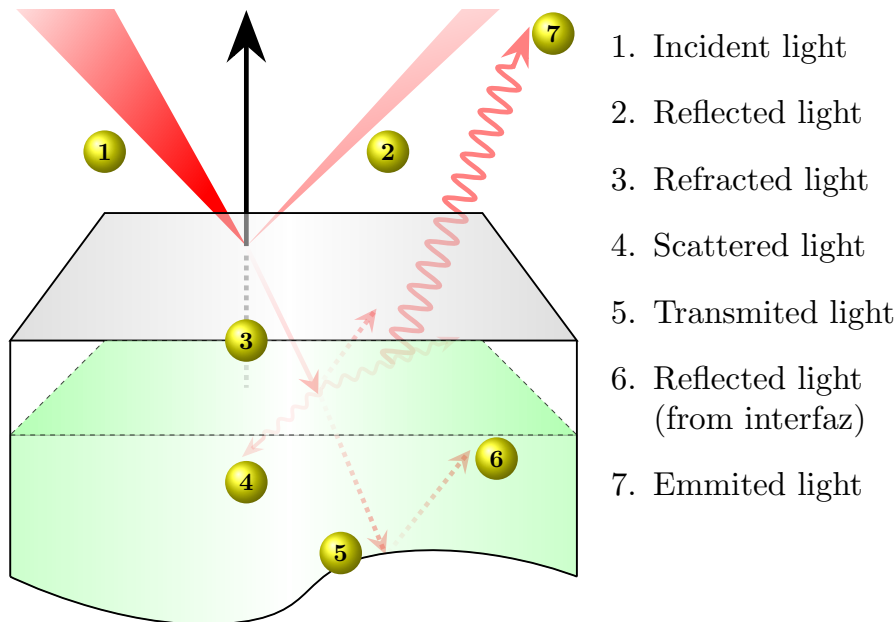


Figure 3.3: Processes that occur inside a solid in the light-matter interaction phenomena.

Before continuing with the manuscript of this chapter, I would like to mention that the experiments could not be carried out without the development of detectors, specifically optical detectors. To speak about optical detectors, it is impossible not to mention the

*Refers to light due to radiation spectral range

photoelectric effect that in general terms is the transfer of energy from photons to electrons when the light spot on a surface [53]. So, this fundamental quantum phenomenon is the basis of detectors in spectroscopy, these detectors are called photodetectors, where these convert the light power(photon incidence over their sense area) into an electric signal, voltage, or current, then this signal we can measure and amplify it. The next sections will mention and discuss the PD implemented in the experimental setup and especially which are the pros and cons. It is important that the photo-cathode of the photo-detector corresponds to the spectral range of experiments. i.e, in our experiments the spectral range of interest is from 700nm to 900nm the PD should have characteristics to adequate of this range. The Table 3.2 shows some PD and their characteristics [4].

cathode	range (nm)	ϕ (%)	λ_m (nm)	i_d nA
bialkali (S-22)	300-630	26	400	0.1
multialkali (S-20)	180-800	20	480	0.2
extended red multialkali (S-25)	300-900	7	600	1
GaAs	300-920	15	700	2
Cs-Te	160-320	14	200	0.01

Table 3.2: Photo-cathodes, usually implemented in PD to the spectroscopy of semiconductors [4].

As a comment, it is important to denote that the CCD devices are been span in many setups in recent years and this is because these devices enlarged the range of experiments that can be realized with these, above all in other areas of physics as in the experimental astrophysics in which has obtained awfully important results. Nowadays, CCD devices in experimental solid-state physics have contributed to getting great experiments that previously were limited due to spatial resolution and time response. In the ??, it discusses the advantages and cons of the detectors (PD and CCD) in PL spectroscopy context.

3.2.1 Photoluminescence Spectroscopy (PL)

Photoluminescence spectroscopy is characterized by be a fast spectroscopy to get optical properties (i.e band-gap) and transitions in semiconductor materials, for this reason the work began with PL spectroscopy with aim of searching optical transitions in each CQWs samples and compare with numerical solution of one-dimensional Schrödinger equation (see ??).

Although PL signal is characterized by be greater than other spectroscopies implemented in this work, the need to use a chopper is only to filter the signal to the external noise, this is achieved used a lock-in amplifier where the reference signal is the chopper and signal input is first measured by a multimeter and then input in the lock-in amplifier. In many other experimental setups the experimental measure are take fast, this is because

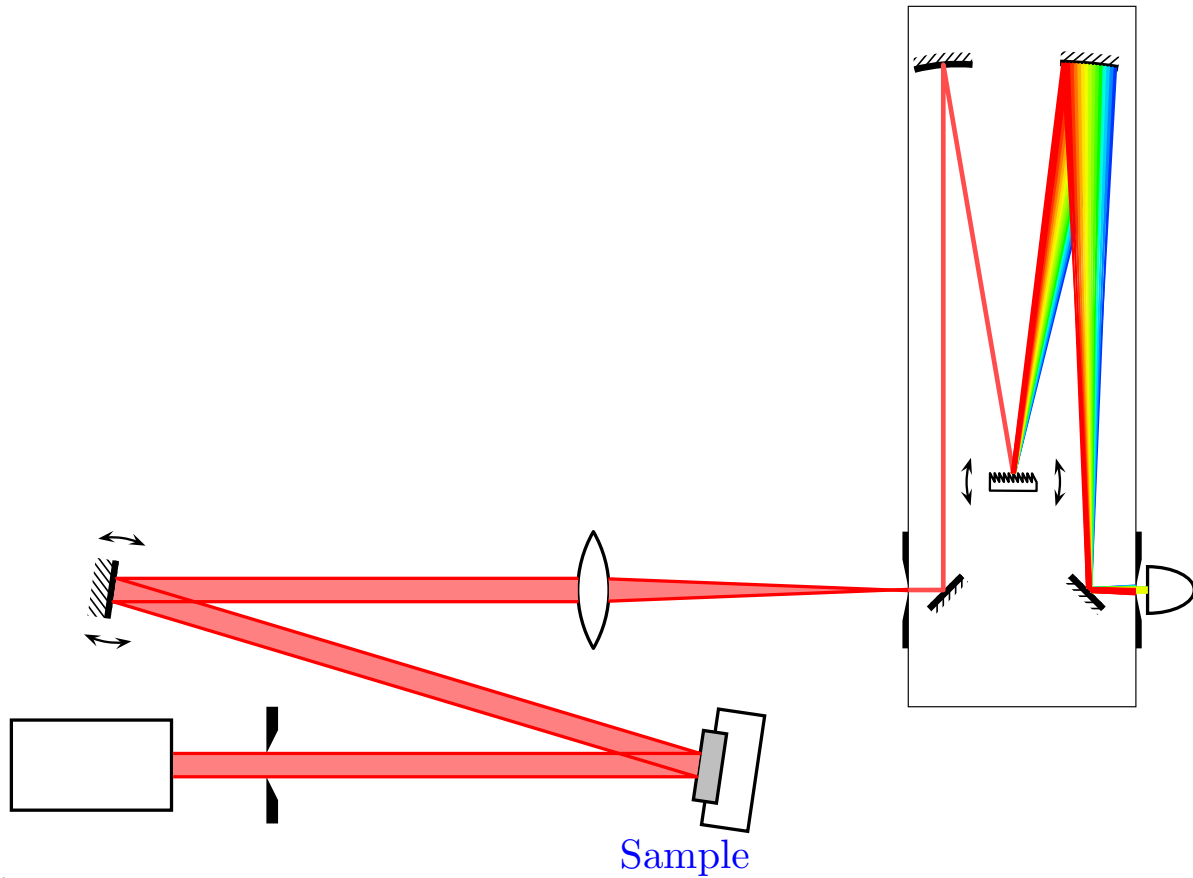


Figure 3.4: Scheme of photoluminescence setup, the temperature of experiments at 14 K, the wavelength of laser 685nm and was used a Si detector.

implement a CCD device as a detector of experimental signals, where these devices are distinguished by fast time of acquisition (apart from other reasons). In our case the time of measure it does not comparable with those, due the time in our experiments is about 2 hours (explained latter) and those are about several minutes. But why use lock-in amplifier if CCD devices shorter measured time?

The answer is not be for impatient*, the reason is that, the lock-in and detector implementation allow control over spectral resolution through two parameters, the first one is in the choice of monochromator's slits apertures and the second one has to do with step wavelength this is the progress step by step over the spectral range taking into account in the experimental measure. Also, the step by step experiments provide the choice of measures number in each step where finally only consider the average of these points, resulting more clean spectra in compare with CCD setups†. Although the time is important worth it inverts to get quality experiments.

*The author self-considered impatient

†Even if modify time and average of measures, the spectra measured with lock-in amplifier are more quality.

Sample	Laser	Range(nm)	λ step (nm)	No. of singnal acquisition	Slits aperature (μm)
M4_3171	680	800-820	0.1	20	75
M4_3172	680	780-840	0.1	15	75
M4_3226	680	800-820	0.1	20	100
M4_3140	680	800-820	0.1	20	100
M4_3141	680	800-820	0.1	20	100
M4_3521	680	800-820	0.1	20	100
M4_3522	680	800-820	0.1	20	100
M4_3526	680	800-820	0.1	20	100

Table 3.3: PL experimental parameters implemented in each sample, all experiments were carried about 14K and was used the same red (680 nm) laser diode. The measured parameters as a Wavelength step or number of acquisitions per step Wavelength were optimized as explains in the text.

Some experiments shown below correspond to Carlos's bachelor thesis [54], who implemented a simple and reliable PL system also he makes a computational code to fit PL spectra using numerical and experimental results (you can check Carlos's codes in our laboratory repository on GitHub*). These results were correlated with previously realized experiments taking into account the same parameters.

The experiments are organized by labels, how shows in Table 3.1, started with the samples M4_3171 , M4_3172 and M4_3226 where these samples were grown with objective the measure trions. The experimental parameters are shown in Table 3.3, in each experiment the optical setup was optimized to enhance the signal measured, the optimization process consisted in measure laser peak at a definite monochromator slit's aperture then finely move the mirror until achieving a high response in multimeter, repeat this closing the slit's and measuring the FWHM of the laser peak in each step, finally we obtained an optimal resolution about 1 nm in our PL experiments.

An important detail about module laser ThorLabs and very remarkable in the ?? is related to power, the power of this was not stable in some time periods causing a variation in the results, this is the reason to use different experimental parameters and after some test were optimized the choice of the Wavelength step, number of acquisitions per λ step and slits aperture, this depending on each sample.

The PL spectra, corresponding to the samples showing in Figures 3.5(a) and 3.5(b), were more complicated to interpret and in experimental conditions as well. For this reason, we decided to calculate the absorption along of the structure that composes each sample because due to they have more layers. We speculated that this is the reason why it was complex to realize the experiments and their analysis. As previously spoken, the study of light-matter interaction in solids can be a headache this is because

*<https://github.com/Spectroscopies-Lab-IICO>

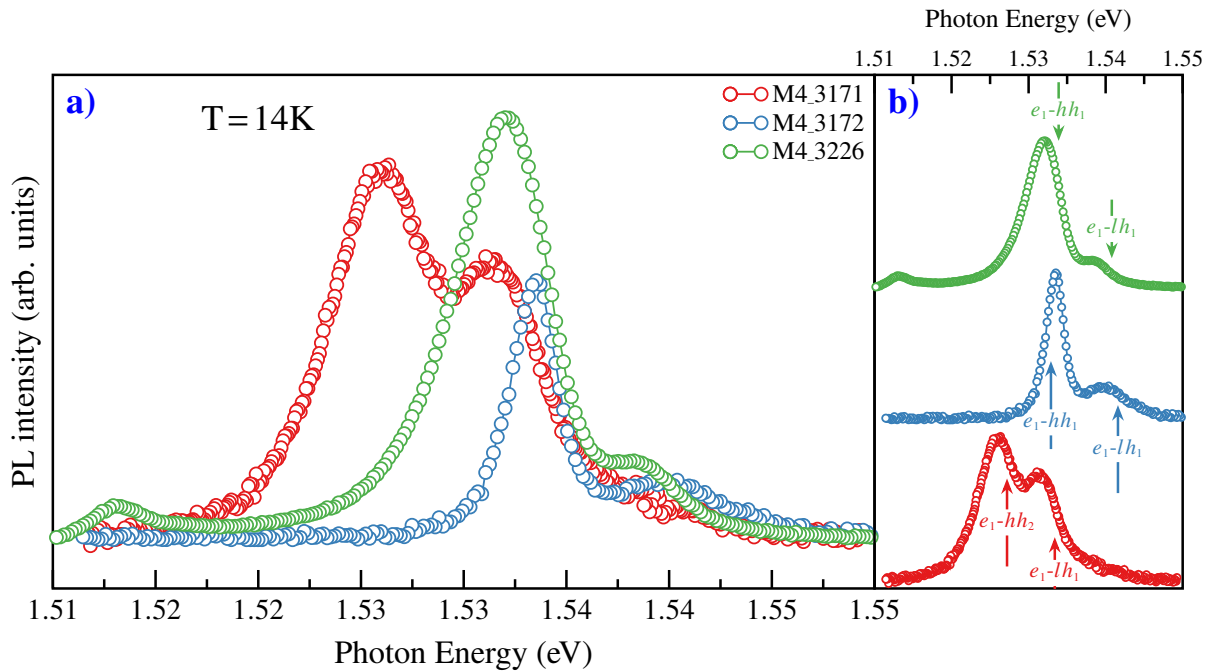


Figure 3.5: Subfigure (a) shows PL experiments of the samples M4_3171 , M4_3172 and M4_3226 , where show spectra and results measured at 14K. Plots in how the comparison between these samples, where clearly can see the relative intensity among in each experiment. In (b) it can be seen each PL spectra with the respective direct transitions numerically calculated, hh1 and lh1 indicates the first energy level that corresponds to heavy- and light-holes respectively.

in real experiments more than one interaction mechanism can be observed, especially in PL spectroscopy and, the objective is to measure only one of them, therefore, the experimental results can be affected and complicate their interpretation. The reason for starting with the samples of Figure 3.5 is that they have effects that modify the PL spectra and, although these effects are very interested in our case, they reduce the PL signal.

If started with the scoop, that the PL spectrum in semiconductors is given by an interband emission generated by recombination carriers, and this, in turn, is due to the absorption of photons provided by an excitation laser source. Therefore, the PL signal is due to absorption, it does not matter that they are opposite processes, the absorption, as well as many other mechanisms of light through the solid, can modify and generate the spectrum of PL. The absorption analysis was carried on in the macroscopic approach to light-matter interaction (in Chapter 4, talks about quantum processes and aspects of light-matter interaction in a microscopic environment), therefore, can use classical electrodynamics to study optical properties of semiconductors. One crucial property of semiconductors is the dielectric function, this is proportional to the complex refractive index (later it is named only as refractive index) and with this, can be described the optical properties of

semiconductors. It is important to mention that the refractive index describes how light propagates in a medium, and it expressed as [?, 55]:

$$\tilde{n} = n + i\kappa = \sqrt{\varepsilon(\omega)} \quad (3.1)$$

where the real part (n) represents the refractive index and the imaginary part (κ) is the extinction coefficient. Even if the objective of this work does not rewrite and reinterpret the physics of these phenomena, we will try to focus on specific equations to reach the goal, which is the absorption model in semiconductors. Then the electric field inside a solid can be written as [55–57]:

$$\mathbf{E} = \mathbf{E}_0 \exp\left(\frac{-\kappa\omega z}{c}\right) \exp\left(-i\omega\left(\frac{nz}{c} - t\right)\right). \quad (3.2)$$

In the Equation (3.2), can see the solution of Maxwell equation in a macroscopic picture of the photon-material interactions. This represents a wave propagating with dispersion and staying in terms of refractive index, but the principal idea is to establish a relationship that can help us to describe the absorption in terms of these principal parameters. The absorption is a process that occurs in any spectroscopy and is the absorption coefficient that defines such a feature in each medium. The extinction coefficient κ is the cause of the wave damping when the electromagnetic wave crosses in media, therefore it's related by absorption coefficient. Now in Figure 3.3 can see that there are three principal parts, that they are intensities that are reflected, transmitted, and absorbed. These three parts compose the original incident light through:

$$I_0 = I_R + I_T + I_A \quad (3.3)$$

Finally, we call upon one of the most notable laws in spectroscopy, this basic expression relates the intensity of light absorbed with the absorption coefficient and is known as Beer-Lambert law [58, 59]:

$$I(z) = I_0 \cdot e^{-\alpha z}, \quad (3.4)$$

then this tell us how intensity decrease as a function of absorption coefficient. As a result of these basic principles in a real structure, we can define de absorption in each layer. After these general and quick basics of the macroscopic basis of light-matter interaction, let's move to a more realistic environment where the calculations are more complex and where it is decided that parameters have major physical priority. The numerical solutions of absorption along structure were carried out using an exceptional Open-Source code

called **SOLCORE** [6]* and our codes. As previously mentioned in a real calculation is frequently taken into account only parameters with major physical sense depending on the situation, arduous computational solutions, or for simplicity. From **SOLCORE**, we have the simplest model to calculate the absorption, despising all reflections at the interfaces having only the absorption as a function of wavelength and depth z expressed as:

$$A_n(\lambda, z) = \alpha_n(\lambda) \exp\left(-\sum_{i=1}^{n-1} \alpha_i(\lambda) d_i - \alpha_n(\lambda) (z - z_n)\right) \quad (3.5)$$

where α_n is the absorption of layer n , d_i is the thickness and z_n the position of beginning of the layer[†].

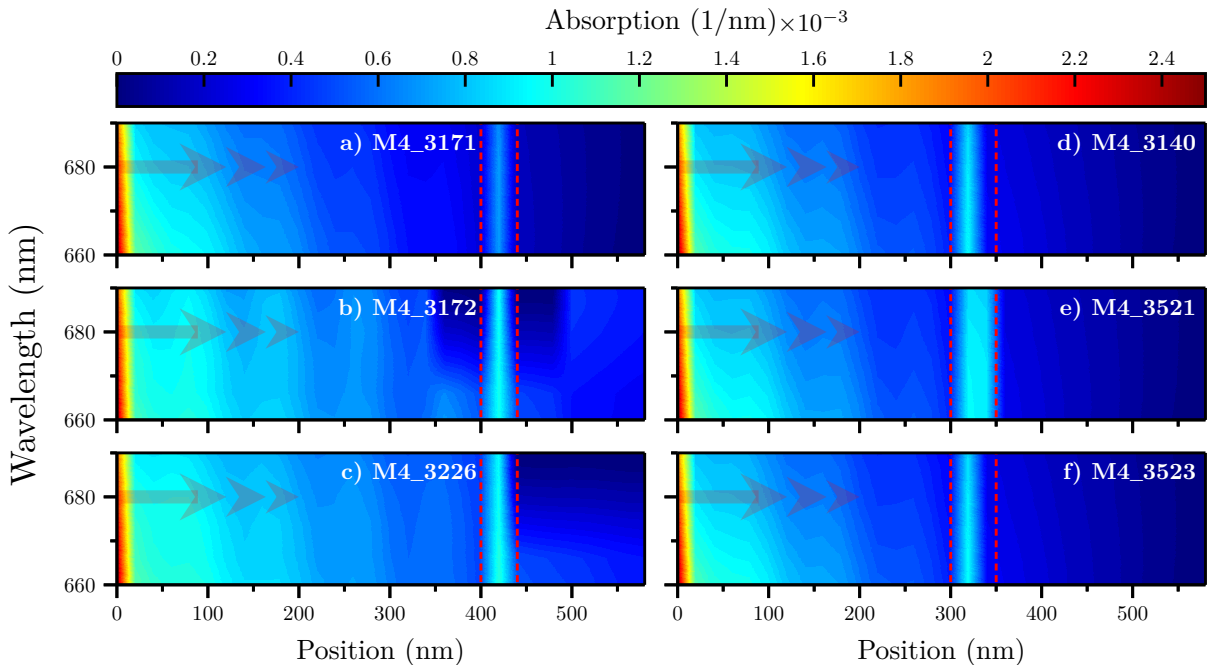


Figure 3.6: Absorption calculated as a function of sample depth, dashed lines closed the CQWs region, left: Figures 3.6(a) to 3.6(c), here the samples have $\text{Al}_x\text{Ga}_{1-x}\text{As}$ layers with different compositions $x = 0.15, x = 0.2$ and $x = 0.3$ this results in a change of refractive index then also expected in absorption. Right: Figures 3.6(d) and 3.6(f) and ?? these samples are equal in structure but change the width of one OM4a)f the QWs, therefore the absorption manifests more homogenous than the first three samples.

The samples with extra layers have characteristics that don't present in samples with fewer layers, one of this is which the fundamental transition around the GaAs gap doesn't

*You can test and contribute this code, visiting their GitHub repository at <https://github.com/qpv-research-group/solcore5.git>.

[†]In eq. (3.5) originally the thickness is represented how w_i , by confusion issues it was decided to change the notation.

possible to observe in these samples, the amplitude in these samples in comparison with sample M4_3141 for example, is around of twenty times smaller than this, opposite case in samples M4_3140, M4_3421, M4_3523. We take these samples because these are the basis of this work, the complete set of PL experiments corresponds to the work previously mentioned. So, why is the important to get the PL results and calculate absorption? The answers are simple, the importance to get PL spectra to help us to get experimentally energy transitions, which have a very important role in the next experiments and in the basis of our model to explain the increase in anisotropy in the ACQWs. Also, the experimental PL results are the basis to compare that our numerical calculations are consistent with the experiments. Numerical calculations get more complicated in large structures, this means, while the structure is conformed with more layers and these layers are thicker, the probability to get a divergence in calculations is great, this is the reason which not all models work. In fact, in our numerical calculations the energy transitions in samples with more layers (M4_3171, M4_3172, M4_3226) we had to be careful at the moment to choice energy binding, the reasons are many and in the PL is complicated to get unique information and even less in structures with high doped, the charge recombination they play us dirty to understand the results.

The case of absorption calculations is a guide to explain the difficulty to carried out PL experiments and put to discussion if doping is a reason to generate or not intrinsic electric field, after all the absorption is part of field solutions.

Figures 3.6(a) to 3.6(c) are the calculations of absorptions as a function of depth, where previously explained, it was only taken into account classical regime therefore the absorption remains in terms of the optical parameters of each layer which conforms all structure. In these figures can shows that in a range of 650 nm to 700 nm the wavelengths are absorbed with major proportion in the first layer, this is due to the structures starts with a GaAs doped(n- or p-type) or undoped layer. After along in structures, also can observe the decrease absorption to short wavelengths, and the notably increased around of the coupled quantum wells. These calculations make sense in the next section where PR spectroscopy is a powerful tool that can used to measure the optical properties due to the modulation without external perturbation, this means that the modulation depends on the intrinsic properties of the structure. The generalizability of the results is limited by the classical regime, as previously mentioned, it has taken into account the refractive index where the absorption can obtain from the complex part of this, that is the extinction coefficient. The common use of the PL is to determine the band gap and optical transitions in semiconductors, especially in QS as quantum wells, but what happens if consider PL regardless of the penetration depth? In our case it is important doesn't, due to the structures studied have wide layers before of coupled quantum wells region, this can observe in figure 4 where shows the results of samples: M4_3171, M4_3172, M4_3226, M4_3140, M4_3521, and M4_3523. In the PL experiments carried out here, it was used as a show in Figure 3.4 a red laser diode of $\lambda = 685$ nm, although the laser energy is chosen

in respect to energy gap therefore short wavelengths are preferable but how we can see these wavelengths are absorbed in the first layer due to the samples ends in a GaAs layer, even the laser used is absorbed in large proportion. Contrary to the samples measured

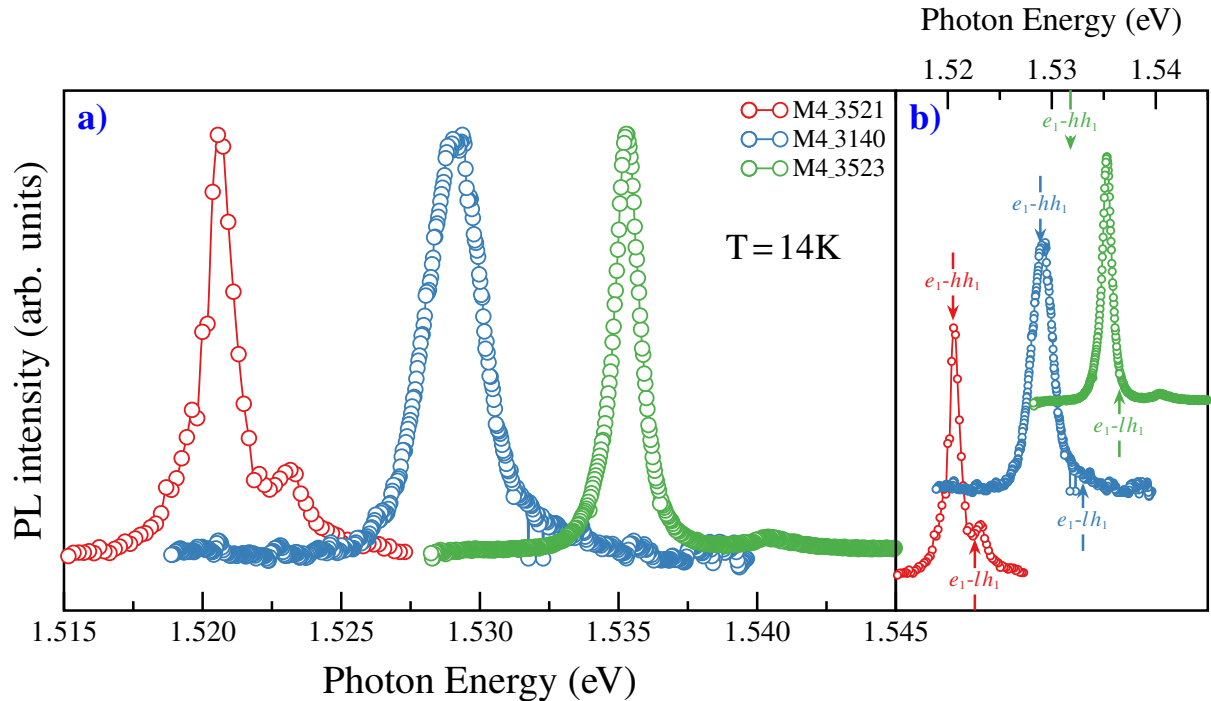


Figure 3.7: (a) Shows the PL spectra to samples M4_3140, M4_3521 and M4_3523, in this comparison is clear the shift between these in respect to first transitions. The relative change in width of one of the QW modify the energy transitions being the sample 3521 the lowest energy. (b) It is plotted each PL spectra result with the correspondent $e_1\text{-}hh_1$ and $e_1\text{-}lh_{1m}$ transitions energies.

first, the samples M4_3140, M4_3521, and M4_3526 exhibits the most spectral resolution this means that exhibit a more homogenous behavior due to the QWs have quantized energy, therefore, the electron-hole recombination is more probably to measure than the other samples which present width spectrums so that these results may be due to the several internal mechanisms of which can be: impurities, large carrier density due doped, defects, among others [60, 61]. In each of these PL spectra, Figures 3.5 and 3.7 present the most intense peaks associates with heavy- and light-holes exciton transitions denoted by $e_1\text{-}hh_1$ and $e_1\text{-}lh_1$ respectively. In discussion with the aforementioned mentioned, several mechanisms can contribute to getting an inhomogeneous spectrum, even it can say that the two peaks which correspond to exciton transitions are thick and merge this can be related with the high doped level this is because very high dopant concentration causes an overlap of the impurity band with the free-carrier continuum [61]. Table 5 shows the comparison between experimental transitions energies get with PL and the numerical results. It is important to mentioned that the approximation of numerical calculations are

closed to experimental, the difference is about of 5 meV for the PL case. It is well-known that the PL signal is increase as a function of decrease well widths, as shows

Table 3.4: Comparison table between experimental transitions obtained trough PL measures and numerical transitions calculated as explained in ??

transition		M4_3171	M4_3172	M4_3226	M4_3140	M4_3521	M4_3523
e1-hh1	(E)	1.5270	1.5341	1.5329	1.5170	1.5207	1.5354
	(N)	1.5313	1.5342	1.5339	1.5292	1.5196	1.5354
e1-lh1	(E)	1.5318	1.5402	1.5286		1.5234	1.5406
	(N)	1.5370	1.5414	1.5408	1.5335	1.5220	1.5366

Table 3.4 shows the comparison between experimental transitions energies get with PL and the numerical results. It is important to mention that the approximation of numerical calculations is closed to experimental, the difference is about 5 meV for the PL case. It is well-known that the PL signal is increased as a function of decrease well widths, this due to the energy of the confined particle state depends on strongly in it and this is demonstrated in Figure 3.7 this due to structures doesn't have top n-type epitaxial layer these structures are i-n type, staying only barriers structures and PL line shape presents strong confinement [62–64].

3.2.2 Photoreflectance spectroscopy (PR)

POTOREFLECTANCE belongs to the group of modulation spectroscopy, being one of the most important to determines field effects without external perturbations, this means that there is no need for an external source that generates the electric field on the sample. Exists another's kinds of modulation spectroscopy, where the type of modulation depends on interest effects, these can be phenomena linked with temperature (thermoreflectance), strain (piezoreflectance), electric (electroreflectance), etc. There is a great information amount of based on this technique, so it decides as previously mentioned and not to repeat in future chapters or sections, the principal idea is to focus on more representative expressions and phenomenological interpretation which be the best following our models and results. Unlike the PL the PR is the reflectance measure as a function of modulation or the changes in it, this once more needs to involve optical properties of the sample studied, in the eq. (3.1) is expressed the refractive index with their real and imaginary part respectively and these are proportional to dielectric function. If the PR is the change in R which is due to modulation of an intrinsic electric field generated by doped layer o layers in the sample (later discuss this mechanism) this mean that:

$$\frac{\Delta R}{R} = \frac{R_{\text{off}} - R_{\text{on}}}{R_{\text{off}}} \quad (3.6)$$

where R_{off} and R_{on} are the reflectivity when the perturbation (laser) are activate or not are the reflectivity when the perturbation (laser) are activated or not, this mean that the results falls on perturbation that is the laser.

The PR as modulation spectroscopy is a powerful tool to perform the study of semiconductors, their modulation mechanism occurs when the built-in field is screening by photoexcited carriers created through incident photons, which involves contactless and non-destructive. In many cases, this spectroscopy technique is preferred due to it can measure transitions in heterostructures at room temperature in comparison with the PL or PLE [65] that are measured at low temperature. Therefore, the highlighter characterize of the PR is the modulation of the built-in electric field, in part, this is due to the structure characteristics but in fact, the PR spectra is the change that generated electric field in the dielectric function, this is expected because is the result of measured the changes in reflectivity generated by the laser, in other words, the laser induces an excess of carriers which neutralize intrinsic field. This is well-known to study in the bulk materials, the models show as the reflectivity change is very well approximated by a first-derivative [66–69] but in QWs structures that are dominates by excitonic transitions then the PR line shapes can be understood in terms of modulation of dielectric function appropriate for excitons [65, 70–72].

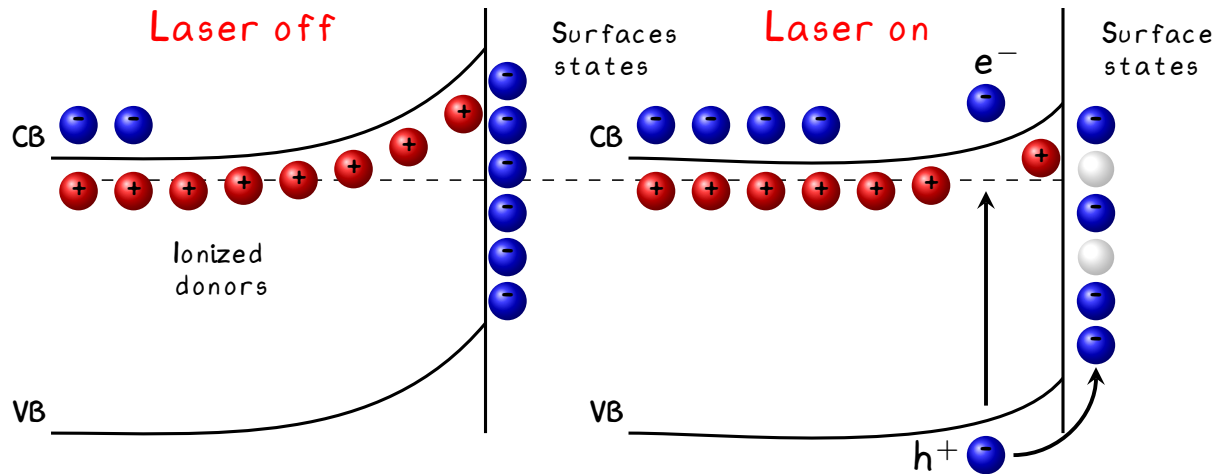


Figure 3.8: Scheme of the PR effect where it shows the carrier dynamics, in left can see the photoinduced changes by the laser is applied.

Under the objective of this thesis, we have not focused on doing a traditional study of the line shape with their respective model, the study over PR lineshape is complex, the interpretation starting from changes in dielectric function like a derivative shape and depending on magnitude perturbation, i.e, doesn't is same the PR analysis on structures with free carriers in solid that the confine particles in QWs structures, the bounded particles are not accelerated by built-in field modulation, so the energy spectrum is discrete and not continuous like free particles. The capability to implement a lineshape fit, do the PR be a great tool. It has been mentioned which the photoreflectance process is due to the

built-in electric field modulation, therefore we are considering that the sample was grown considering desired characteristics to generate an intrinsic field, this means that sample contains n-type doped layers, impurities, unintentional strain mechanisms which generate a space charge region. In the case of an n-type doped layer in a structure, create a space charge region, this region creates the field therefore the conduction and valence bands are bending as is shown in the Figure 3.8 and the Fermi energy are pinning at the surface. Photoexcited electron-hole pairs are separated by the built-in field, with the minority carrier (holes in this case) being swept towards the surface.

At the surface, the holes neutralize the trapped charge, reducing the built-in field [68]. That is the general explanation to the PR modulation, before we mentioned that a characteristic of the PR, is to fit as a derivative-like and the order depends on structure, also, we mentioned which in quantum wells the confinement and bound states modify the line shape and the respective fit. So, in this situation, the modulation of field causes the binding energy change of excitons, in other words, this is a Stark effect but in an inverse case because of the field it already exists. The electron-hole pairs depend on binding energy, if that is modified, then the intensity of the transition varies.

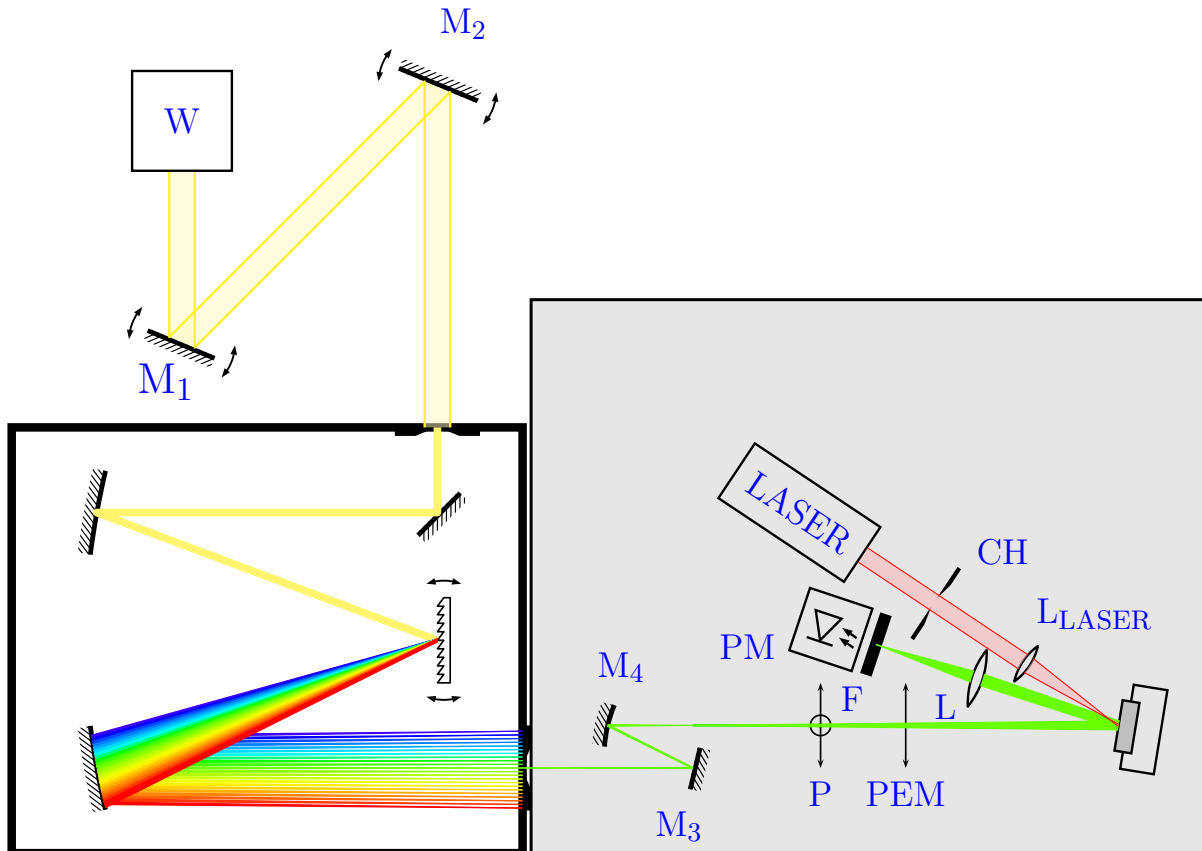


Figure 3.9: Photoreflectance setup used in these experiments, the setup implemented is commonly called dark configuration this due that photo-detector are exposed, then keeping closed to ambient light. W: tungsten lamp, M₁ to M₄ variable mirrors, P: polarizer, PEM: photoelastic modulator, L: focus lens, F: filter, PM: photomultiplier, L_{LASER}: focus lens for laser, CH: mechanical chopper.

The experimental setup to PR experiments implemented in this work, shown in Figure 3.9. The setup start with the probe light from a tungsten lamp, the beam is led by two silver mirrors to monochromator entrance slit, then the monochromatic beam passes through a polarizer and a photoelastic modulator finally affects on sample. The reflected light is focused to the PM with a focus lens. Modulation of the electric field in the sample is caused by photo-excited electron-hole pairs created by the pump source in our case is a red laser that illuminates the same spot of the monochromatic beam and is chopped to a certain frequency, in this setup we use a mechanical chopper at 1KHz. It is important to mention that the reflected light in addition to being focused by a lens, is filtered before incide at PEM, this is important because the reflected laser light by the sample can modify the modulated R signal, do not forget that the PL signal is involved too.

Although the R signal is modulated by the chopper at 1KHz, after is measure by a lock-in amplifier due to the change in the R is very small about of 1×10^{-4} , in comparison with the PL signal, R change is less than PL as one million times. This is the reason by which any modulated spectroscopy commonly uses a lock-in amplifier. In our case, the setup is called Dark [68] setup because the PM is exposed to room light, therefore the system is keep closed. The Dark configuration has some advantages, one of these is, that the R changes are subtracted intrinsically therefore the use of the filter is enough to the dispersion of laser isn't a problem. We refer intrinsically to the R signal modulation. If the PL signal achieves to be detected, the system will perform subtraction as shown in Equation (3.6), if the PL signal mixes with the R in both cases this will cancel because it is constant, staying only the change in R.

The result of PR signals associated with band to band and quantum level transitions, in case of samples M4_43171, M4_43172 and M4_43226 the built-in electric field is low due to the structure n-i-n, this in principle is canceled or screen, this mean that the field create by carriers is opposite. The Figure 3.10 shows the result of PR experiments on samples mentioned above and are a bit informative. In fact, GaAs gap isn't visible in these samples, many mechanisms can affect the PR results in these. The first one and more representative undoubtedly is the low built-in field, if the structures are n-i-n the field expected is so low although the field can affect the interfaces and contribute but in general this is cancel by opposite photo-carrier directions. Frequently the PR is used tool to calculated or estimate intrinsic fields, this is possible in intermediate-field regimen, this known as Franz-Keldysh oscillations (FKOs) by electric field along z -direction [73]. So, the in PR spectra is observed oscillations and the period is determined by the field in the structure, where typically only about 3-4 FKO can be detected in the space charge region of a doped sample. In this case for these samples and as will be explained later, the PR experiments are complex in context to determine all transitions that occur in them and the field is smaller, therefore does not are candidates to have FKO.

The samples n-i-n type as shown in the Figure 3.10 the FKO does not exist and this is clearly observable because these experiments does not have any oscillations, as before

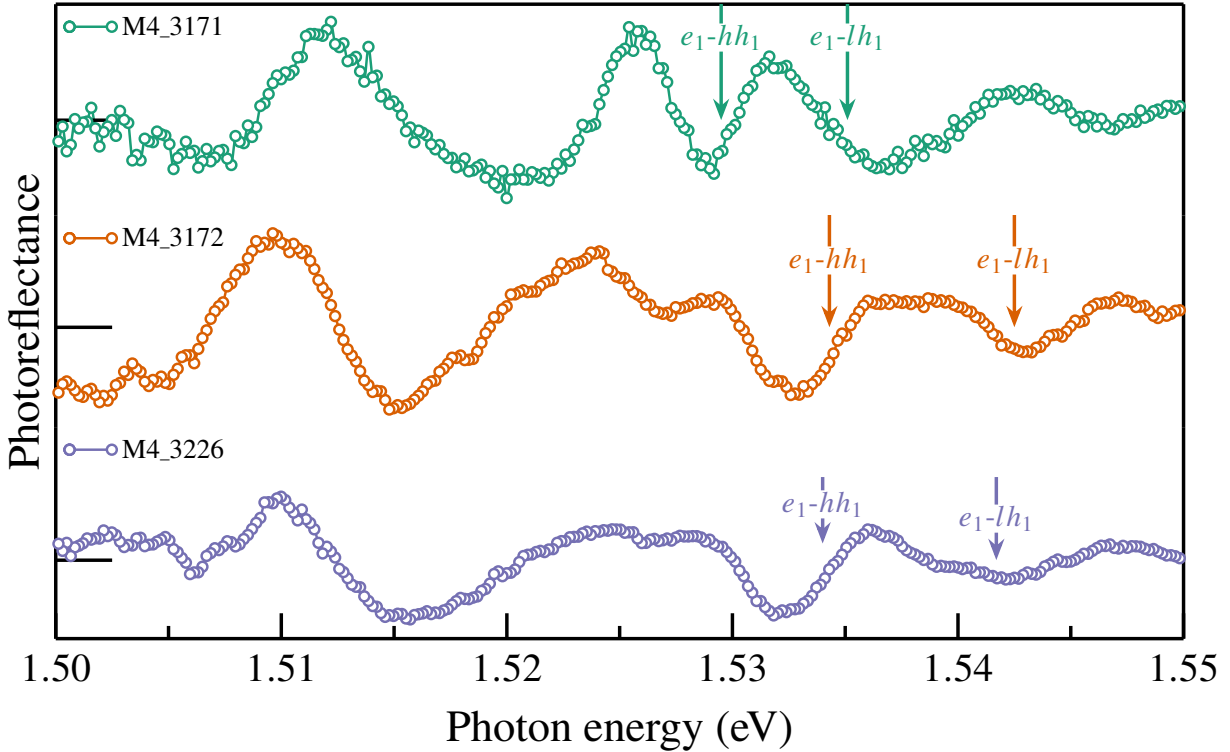


Figure 3.10: PR experiments to samples: M4_3171, M4_3172 and M4_3226 at 30K. Arrows point to calculated transitions for each sample, the used laser wavelength was the same, which in PL experiments and the power used in each of these was 5mW. Dashed line point the GaAs substrate.

mentioned this behavior may be occurred because the directions of photocarriers generated are opposite, then the intrinsic field is canceled. Thus, the PR measured spectra are the result of modulation of intrinsic residual electric field or nonuniform fields effects [74]. In contrast, with the n-i-n type samples, the i-n type samples exposes clearly the direct transitions even associated to transitions with more energy (next levels energies), although the intrinsic field is not enough to generate FKOs.

In the Figure 3.11 can see the direct transitions numerically calculated for samples M4_3140, M4_3141, M4_3521, M4_3522 and M4_3523. The sample M4_3521 was taken as reference in terms of amplitude, in the sample M4_3140 was performed experiments as a function of power laser, being the power 2.5 mW the closest at 5mW, this is one of the reasons for that the result spectra was approx four times smaller than the sample M4_3521. The sample M4_3522 p-type, maybe can be five times smaller than their n-type analogous sample (M4_3521), but the line shape resultant does not have any response, i.e., in terms of amplitude is smaller, but the transitions aren't clarified or not resolved. This is one of our keys to final results because it has to do with carrier distribution and the nonexistence of the built-in electric field. For the sample M4_3141 the PR spectra is similar to the sample M4_3140, the difference between these structures is the barrier width, but in spectra the

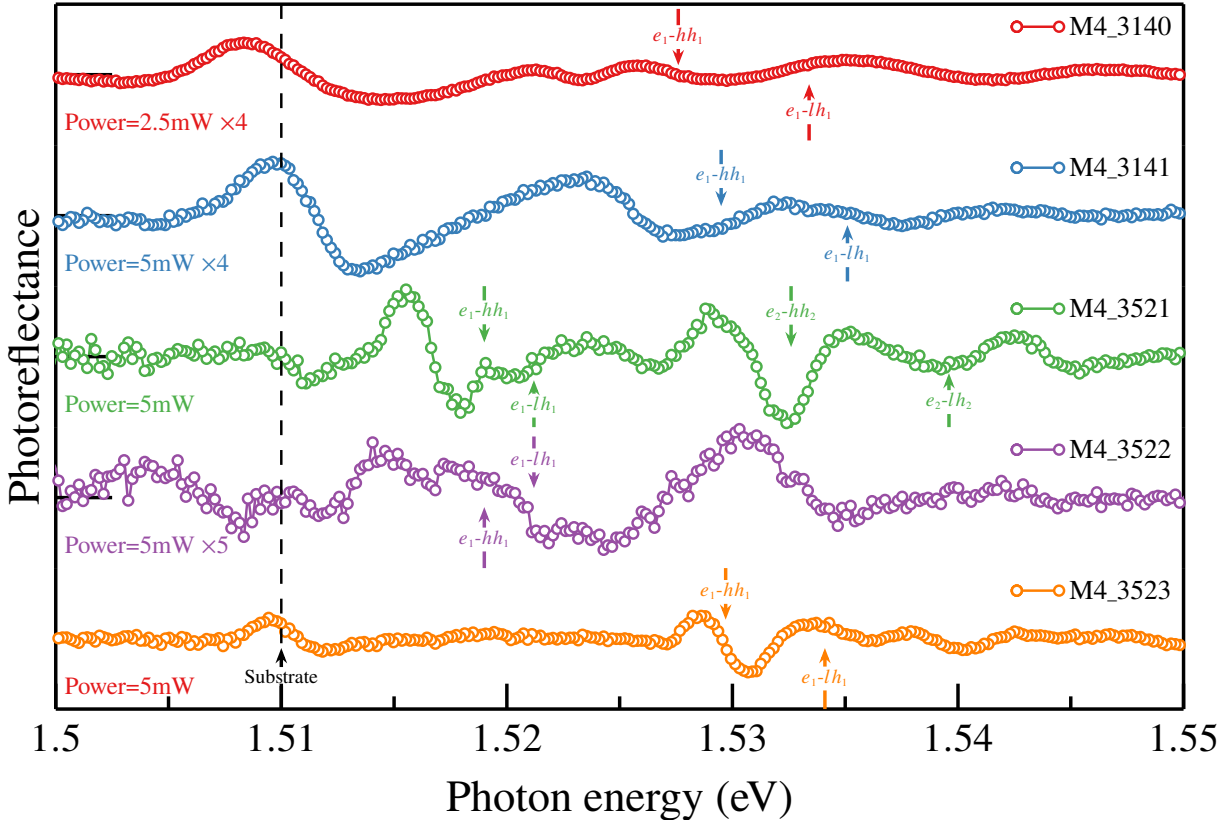


Figure 3.11: PR experiments to samples: M4_3140, M4_3141, M4_3521, M4_3522 and M4_3523 at 30K. Arrows point to calculated transitions for each sample, the used laser wavelength was the same, which in PL experiments and the previous PR experiments. Dashed line indicate the GaAs substrate, in these samples this transition is well located. The PR spectra of sample M4_3522 p-type doped (orange) is five times smaller than their correspond n-type, the sample M4_3521. The experiments in sample M4_3140 was performed at 2.5mW, then was multiply it by four in according to samples M4_3521 and M4_3523, in case of the sample M4_3141 even if, was performed at a power = 5mW the result was 5 times smaller than sample M4_3521. The discussion about of this is explained in the text.

transitions are more resolved in the sample M4_3141.

From now on, we focus on the samples : M4_3140, M4_3521, M4_3522 and M4_3523, these samples are similar in structure, if shows experiments of the n-i-n type samples and the rest of i-n type samples is only to remark the importance of our results.

Even though in many works about the PR is normal to submit a line shape fit model to clarify the effects of modulated intrinsic fields around of critical points or transitions and as before mentioned this doesn't the interest of this work. Although, the study and models of line shape for modulated spectroscopy as the PR are essential in the experimental study of semiconductor physics [75, 76]. Nevertheless, in our experiments although the PR mechanism is observable in general around of the Gap (E_0) and direct transitions, the mechanism of modulation over the low intrinsic field, exhibit effects which is not frequently

in the PR experiments, as it's shown in the following section.

3.2.2.1 Excitonic effects

THE CQWs structures are useful to study excitonic effects under external perturbations of an applied electric field. These structures are coupled by the thin barrier, then the electrons overlap over both wells, this behavior is very studied by the confinement effects and possibility to create devices based on electron properties. In this work, we focus on the samples which exhibit exciton effects that commonly are observed under external field apply in our case, without external fields or external perturbations and nor any structure modifies*. Starting with a comparison between ACQWs n- and p-type these are the M4_3521 and M4_3522 samples respectively, Figure 3.12(a) shows the PR of both samples(left), where the p-type sample is approx five times smaller than the n-type sample, therefore we can conclude that the mechanism of photo-carriers generated in these are different even if it has the same CQWs structure.

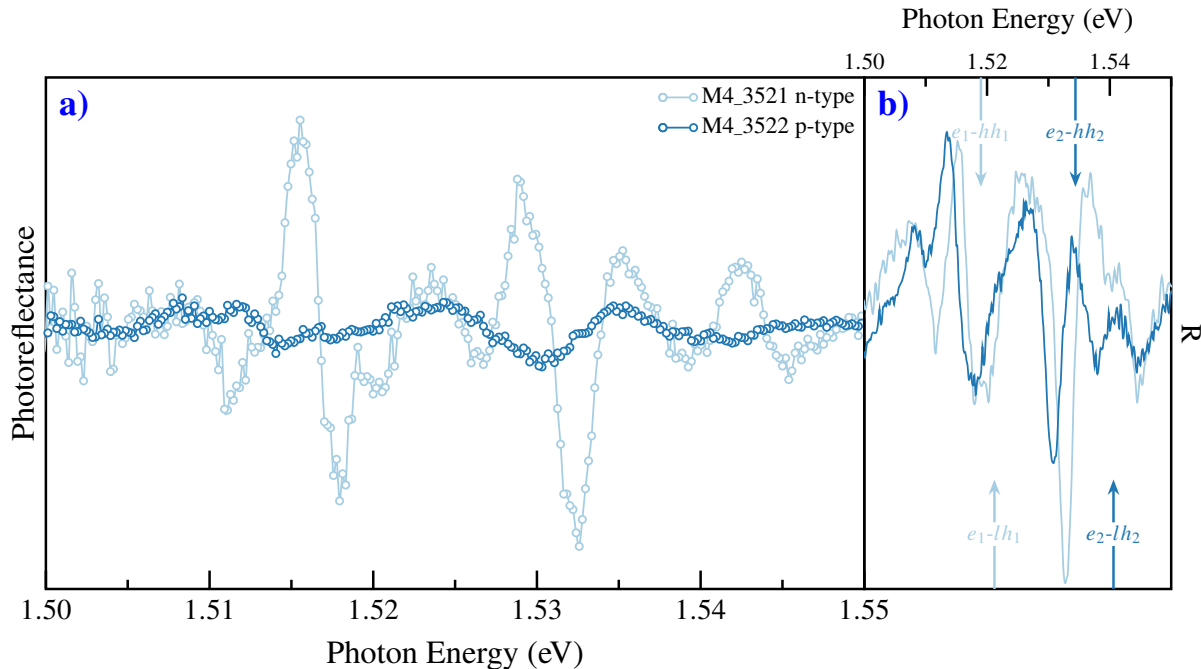


Figure 3.12: Comparison of : a) PR spectra of the 3521 (n-type) and 3522 (p-type) samples, the p-type sample is 5 times smaller than n-type sample. b) R spectra obtained at same time in each experiment, the arrows point to each direct transitions for two first confined energies. The line shape is practically the same in both spectra.

*This refers to create strain by polish over the samples or mechanisms which generates strain, external perturbations also refers to temperature changes, applied currents, and others.

Also, the R spectra as shows the Figure 3.12(b) obtained synchronously at each experimental measured, this is the DC signal detected by photomultiplier and reading by the multimeter. These signals are practically the same, according to equation eq. (3.6) the change originated by the laser source doesn't enough, i.e., $\Delta R = R_{\text{off}} - R_{\text{on}}$ is smaller. In another way, the comparison of samples M4_3521 (ACQWs-2) and M4_3523 (SCQWs), shown in the figure Figure 3.13 exhibits the difference in amplitude at same power laser but around de E_0 is well resolved in both. In case of the SCQWs sample the direct transitions are well resolved, but in ACQWs-2 sample, could be present forbidden transitions, pointed at Figure 3.13 with same color of its correspond PR spectra. This behavior it has been observed previously [77] in MQWs structures even at 300K [78]. The nomenclature to allowed transitions (direct transitions) is: en-hhm for electron-heavy hole and en-lhm for electron-light hole, n index represent the n-th conduction subband and m-th valence subband. So, when n=m its refer to direct transitions or allowed transitions, in ACQWs appear peaks related to transitions between first electron energy where electron wave function is predominantly in the wide well, but this wave function is overlapping to narrow well even if in minor percent, this mean that n \neq m then the heavy- and light-holes confined at narrow well can create e1-hh2, e1-lh2 transitions, or the electrons in second confined energy that predominantly are at narrow well but, they can penetrate (tunneling) to the another well (wide well) as seen in Figure 3.13 can generate another forbidden transitions. It's important to mentioned that this behavior is presented at low-field regime, therefore can't associate this to modulation of the built-in electric field, this being discussed since some years ago [78, 79], even though can this associated, with the behavior which have the electron, heavy- and light-holes in CQWs structures, with a specific barrier width and the height of the potential barriers (or depth of wells) [2, 80]. The electron and holes tunneling depends on those parameters and, in our case, the barriers potential depends on Al percent in the alloy $\text{Al}_x\text{Ga}_{1-x}\text{As}$, therefore $x = 0.15$ then the barriers they are not so tall, and the coupling barrier width is very thin (< 2 nm).

These structures, become an interesting platform to study the phenomenology and behavior of confined electrons, heavy- and light-holes, and their respective interactions. Another interesting phenomenon, which we could observe, was the trions (X^+ or X^-) formation through the PR experiments. When were carried out the set of PR experiments over the samples i-n type, occurred a peculiar event while we performed and established the correct measure parameters, to be specific while we determined the laser power. This doesn't mean that our experiments are wrong, as a matter of fact, this peculiar event made us test the experimental setup several times and carried out experiments as a function of laser power. This event started with the M4_3140 (ACQWs-1) sample, this sample has a well with a slightly wide width and because of that the wave function overlapping in major percent than the others samples, by this reason is reasonable or expected, that the trions formation it's more likely as explain later. While they were being carried out, the PR experiments in ACQWs-1 sample, at higher power laser allowed by our device, in fact,

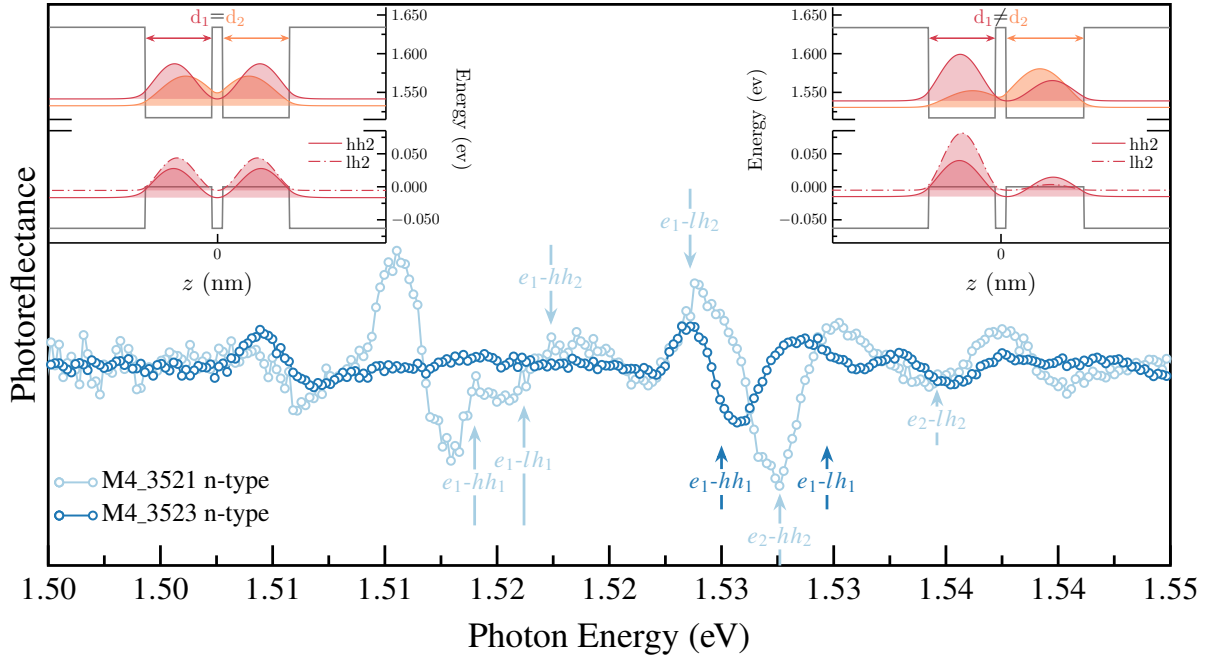


Figure 3.13: The PR comparison between samples M4_3521 (ACQWs-2) and M4_3523 (SCQWs), the electron wave function are plotted for each sample where, the SCQWs sample at top left and at top right to ACQWs sample. The top arrows pointed to forbidden transitions in ASQWs-1 sample, while the bottom arrows pointed to the direct transitions in both samples.

this was trouble, because the laser power doesn't stable, so it was decided to turn on the laser previously before performing each experiment, this was around of eight hours before to start experiments. After detecting the problem with the laser power, it was started the PR experiments at higher laser power, the results were peculiar due to appearing a higher peak with respect to direct transitions, in fact, the direct transitions didn't was observable. These experiments were realized several times and the behavior was kept, then we decided to increase the spectral resolution to try to understand the nature of this peak, previously all experiments were carried out with the monochromator slits at $1500\mu\text{m}$ this to enhance the light collected by PM. The Figure 3.14 shows the evolution of these experiments at $P=50\text{mW}$ as a function of the slits aperture, it's clearly that doesn't about of experimental contraption or another external thing which can contribute or being the cause of this behavior.

From these results it decided all experiments with these apertures of slits, although we try to enhance the spectra resolutions at $750\mu\text{m}$ was they got the best results. In the ?? shows the evolution of the PR spectra as a function of laser power, starting with 1mW of power and finished with 50mW . Remember previously mentioned that the laser power is unstable and this trouble it didn't allow performing the experiments increases power in one way more uniform, this is the reason that the experiments were carried out with powers at 1mW , 3mW , 8mW , 30mW , and 50mW . The spectra with power less than 8mW are relatively similar, therefore, after that power it can see a change in peak width and

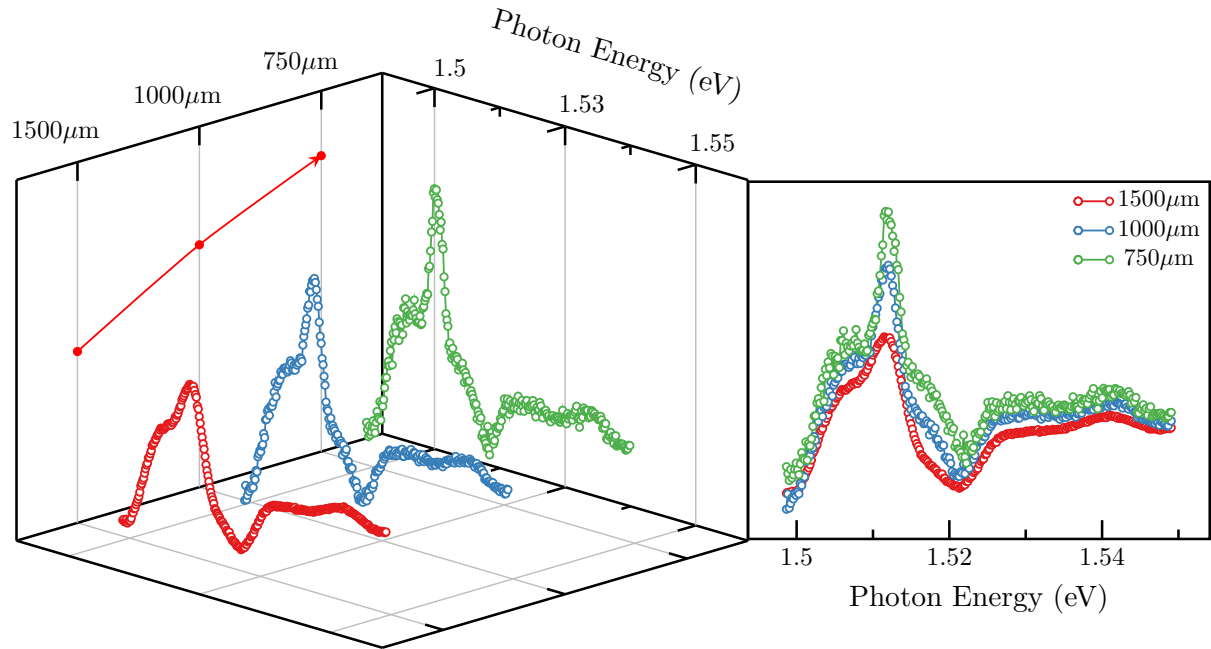


Figure 3.14: PR spectra of the ACQWs-1 sample designed as a function of slits aperture, where it can see the increase of peak resolution as decrease the aperture of slits.

that peak tends to shift at less energy.

Now, we establish the physical background of that rare behavior in the PR experiments. In semiconductors, the electron-hole pairs are the reason for many special phenomena and are commonly called the hydrogen atoms in semiconductors. But to understand the nature of excitons and their consequent behaviors, it needs to start with a specific platform to keep or extend their life and interactions. As above-mentioned, the life of the excitons in QWs is extended for several reasons, of which; well width and low temperatures enhance the binding energy [81, 82]. When the light interacts with these structures, the electron-hole pair associated with the absorption of a photon with enough energy results in an exciton (general explanation), but if inside the structure the electron density is great [83], the excitons and all possible interactions which can occur as exciton-exciton, exciton-hole (X^-), exciton-electron(X^+), electron-electron, even, LO-phonon-exciton interaction. All of this presents in a modification of the line shape resultant, in terms of the PL experiments it's possible to observe unexpected transitions as a slight modification in the line shape. In spite of the physics involved in this mechanism is very complex, the hard work in this theme has generated valuable results.

Since the 50s Lampert [84] suggested the existence of charged excitons also called *trions* in semiconductors and after almost 40 years it's proved experimentally [83, 85], and as expected the trions X^+ or X^- they were observed in QWs. The electron concentration has a role important in trion formation, for this reason, they usually modulated n- or

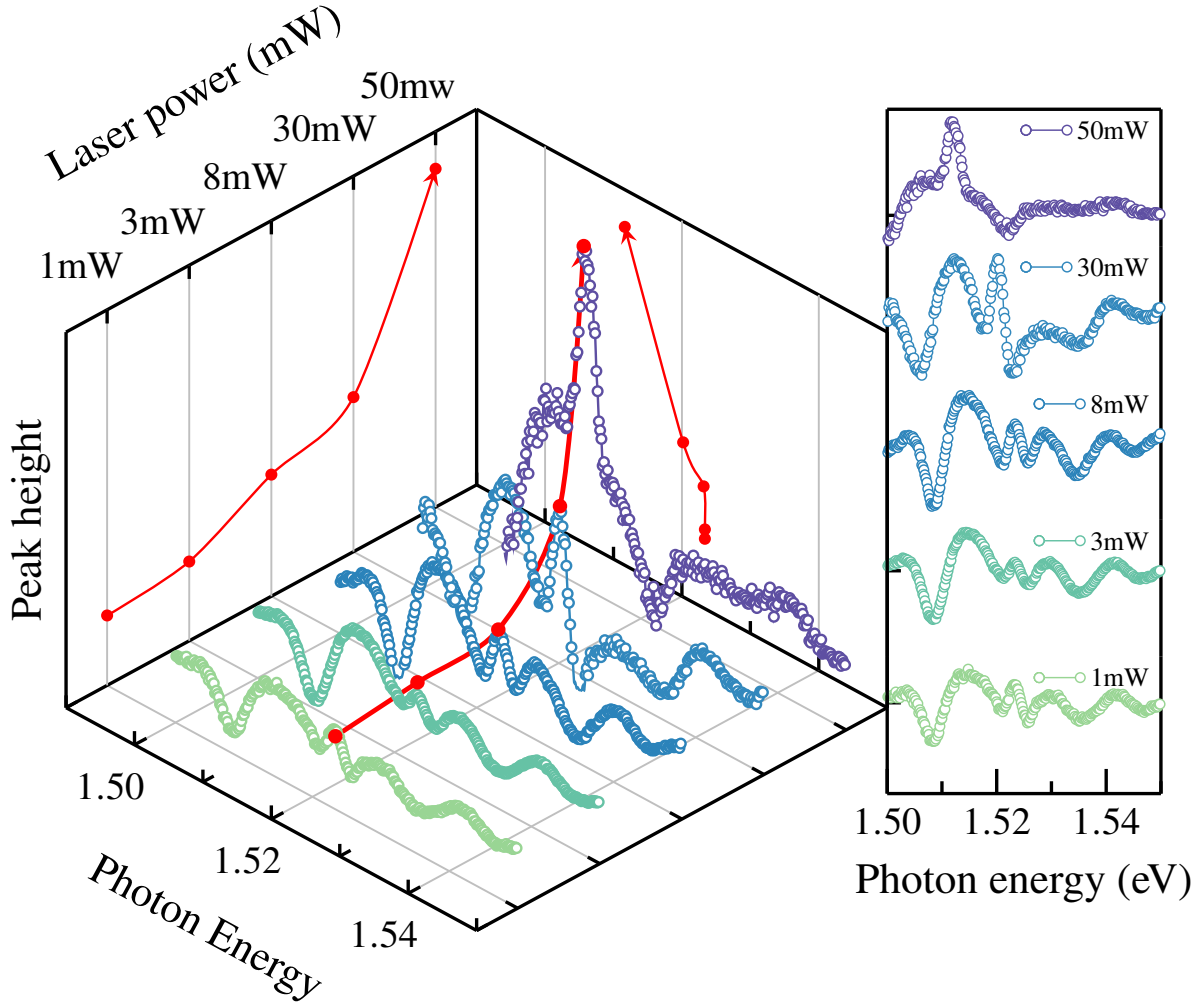


Figure 3.15: The peak tends to height as increase the laser power, which also is very observable as a redshift.

p-type doping in the QWs structures. Also, the external perturbations as the electric* or magnetic fields commonly used to enhance the trions transitions, in the magnetic field case, the trions involved acquiring a triplet state nature, so the Zemman splitting is expected, therefore the transitions are well resolved. At zero field, the ground state of trion is a singlet [86], this is, two electrons with opposite spin, these electrons are bound with a hole as shows the scheme in Figure 3.16(a).

In our case, the trions formation is due to photo-excited carriers induced by the laser source, if we suppose that the doped layer is the absolute answer of this, the other samples

*In this case the trions formation is due a relative position of the Fermi level when the low electric field is applied, in fact, the mechanism involves indirect transitions and is easy that the indirect exciton interact with elctrones or holes [51].

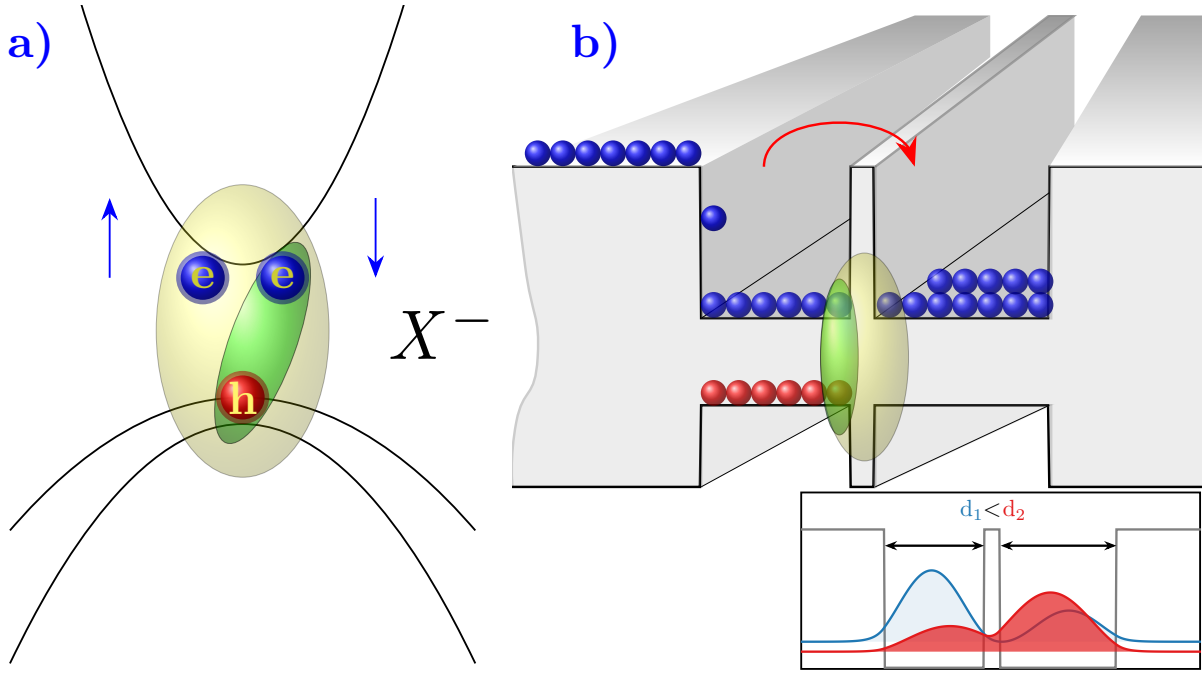


Figure 3.16: Trions formation scheme in terms of band structure (a) in this case, the exciton is bound to an electron in the conduction band leading to a three-body system known as negative trion \mathbf{X}^- . On the other hand, in (b) it presents the possible formation of \mathbf{X}^- due to a slight width of one in the CQWS, consequently, the narrow well transfers electrons through tunneling to a wide well, if it's calculated the wave functions of this structure, the wave functions have the characteristic of to be distributed asymmetrically as in the case of the applied electric field along z [2, 3].

as SCQWS-1 and ACQWS-2 would have similar results in their PR spectra when it increases laser power, but this is not observed, in fact, in these cases the line shape kept but noisily, then if we adjudicate the trion formation to photo-excited carriers, which is the cause that enables trions in the ACQWs-2 sample?. The answer is a hypothesis that needs extra experiments but is part of the future objectives of this work. The electron and holes (hh, lh) wave functions in samples slightly asymmetric in wells widths, i.e., one of the wells is slightly width than the other, these wave functions have similar behavior as the case when de electric filed is applied. This behavior enhances the electron tunneling from the narrow well to the other well (wide well) as shows in Figure 3.16(b), if all-important samples contain the doped layer with the same n-type concentration if we suppose that this layer modifies the Fermi level thus generating a small electron gas (2DEG), its possible think that this electron gas has a function of electron reservoir [87, 88]. Then the photo-carriers generates by the laser source step up carriers dynamics, doing that the narrow well is yielding continuously electrons to wide well through tunneling and, these electrons are recombining with the excitons confined in the plane of the narrow well, therefore results in a three-body system $\mathbf{X}^- = (e, e, h)$ or $\mathbf{X}^+ = (e, h, h)$. As it's known, the trion is a charged exciton where the sign depends on its formation, in the

case of $\mathbf{X}^- = (e, e, h)$ their transition is under the first transition of X_{hh} , and their energy evolution tends to redshift as can see in Figure 3.15. Therefore in our case, which was also has been reported [83, 87–90], the shift evolution correspond to an \mathbf{X}^- trion, however still missing more experiments to strengthen this hypothesis. On the other hand, what happens if the 2DEG doesn't consider? It is very important to emphasize this argument because the objective of this work is to demonstrate that CQWS structures especially ACQWs shows effects of symmetry breaking doesn't see in structures without external perturbation(application of: electric or magnetic field, strain, etc.) or intentional modification (growing of interfaces that unbalance the QWs region, differences in the potential of the barriers), by this reason is importantly empathize that regardless of exist a 2DEG whichever is their electron density and the built-in electric field which can this generate, as a matter of fact, that field doesn't represent the cause of the phenomena presented in this work, more later this is discussed with more detail. On the other hand, is relatively easy to corroborate that the presence of the electric field on those samples can be regarded as despise, what is the reason to asseverate this if the PR has a principal characteristic the built-in field modulation? As before mentioned the non-existence of the FKO's is a point to assert the field regime is low, moreover, in comparison with the n-i-n-type samples, also remain in this regime notwithstanding of be designed to reduce the built-in field. However, it's can be estimated by means of Schrödiner-Poisson, so as to, the equation ?? it's coupled Poisson equation [91, 92]

$$\left(\frac{d}{dz} \varepsilon(z) \frac{d}{dz} \right) V_p(z) = \rho(z) \quad (3.7)$$

$$\left(\frac{d}{dz} \varepsilon(z) \frac{d}{dz} \right) V_p(z) = e \left[n_D(z) - \sum_i n_i^s |\psi_i(z)|^2 \right] \quad (3.8)$$

With the objective of present the behavior and the causes of the high doping in the $\text{Al}_x\text{Ga}_{1-x}\text{As}$ layer, we implement a simple code, starting off our numerical codes and helping us with already implemented codes as Aestimo [7], we calculated numerically Schrodinger-Poisson equation. It is important to mention which solution is self-consistent, therefore the code is implemented with all parameters to divergence avoid, in our case is due to high doping and this is too large.

For this reason, it is inevitable that the codes don't converge, although it can be considered a factor damping to speed convergence [93]. We consider the damping factor, and we decided to calculate a structure as GaAs/n-type doped $\text{Al}_x\text{Ga}_{1-x}\text{As}$ / $\text{Al}_x\text{Ga}_{1-x}\text{As}$, where the width of lateral layers is fixed and the width of the doped layer varies from 15nm to 300 nm with the same n-type doped $6 \times 10^{18} \text{ cm}^{-3}$. In general, the self-consistent Schrodinger-Poisson equation, is a process that starts with the calculation of the confined energies in the potential profile defined as $V(z)$, in this profile are included each parameter of the material that makes up the heterojunction as the doping quantity in each layer

if this is doped. After, as shown in Equation (3.8), is evaluating the space charge with their respective charged donors and their concentration n_D , n_i^s is the electron sheet density of the confined levels and corresponding wavefunctions $\psi_i(z)$. To calculate the electron density in each level i frequently is applied Fermi-Dirac statistics [23, 94, 95].

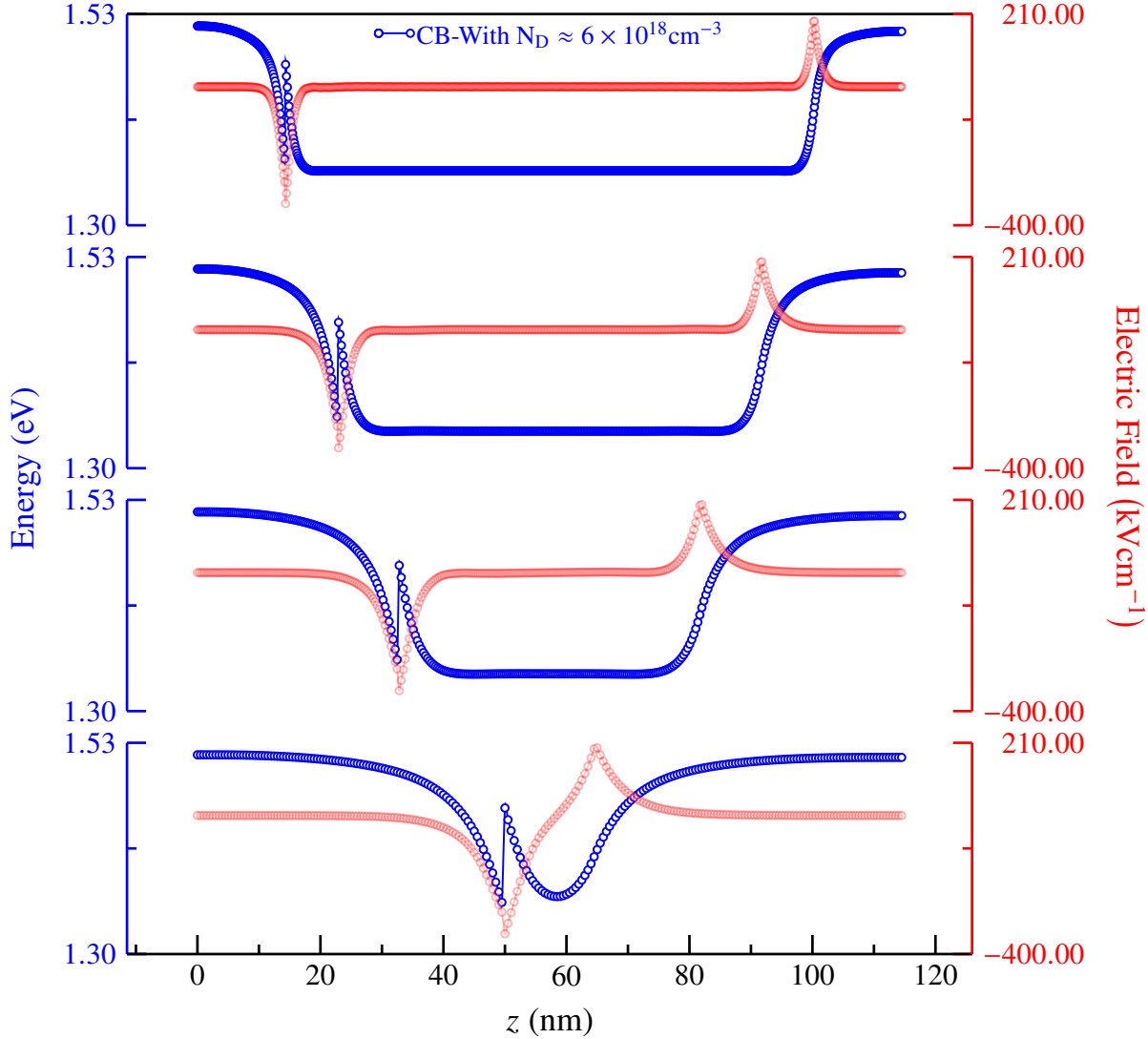


Figure 3.17: Results to self-consistently Schrodinger-Poisson equation, in order with down to top the n-type layer Al_{0.15}Ga_{0.85}As doped ($6 \times 10^{18} \text{ cm}^{-3}$) is increasing in width from 15nm, 75nm, 150nm to 300nm. The goal of this is to calculate in a general way the effects of the doped layer, specifically due to the electric field induced by this. The strength of the field is expressed in kVcm units, although this magnitude is great, we assume that doesn't significantly, latter we explained this.

This charge distribution in the structure gives rise to space charge effects, resulting in an additional electrostatic potential V_p which causes conduction band bending [91, 96]. The total potential V is the result of $V = V_0 + V_p$, where the V_0 is the original potential profile, so, this is the iterative part of calculations, in our case, we established the difference between

$e_{1\text{new}} - e_{1\text{old}} < 1 \times 10^{-5}$ as convergence factor. Previously mentioned the damping factor is defined for fast convergence, in our case α_{damp} is about 1×10^{-3} . The results are shown in Figure 3.17 to a structure : GaAs/Al_{0.15}Ga_{0.85}As(n-type $6 \times 10^{18} \text{ cm}^{-3}$)/Al_{0.15}Ga_{0.85}As with four different widths (15nm, 75nm, 150nm, and 300nm) for the layer doped.

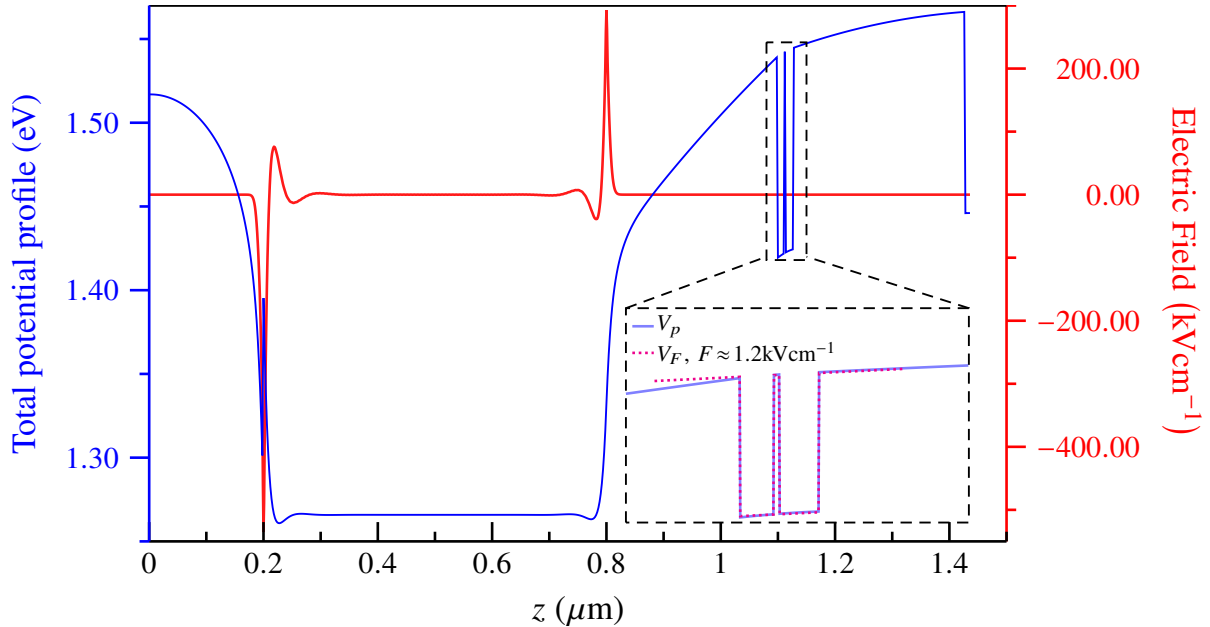


Figure 3.18: Band conduction profile $V(z)$ calculated by numerical solution of self-consistent Schrödinger-Poisson equation. The calculations were performed considering the width of the doped n-type 6×10^{18} layer with 600nm. The zoom inset shows the comparison between total potential calculated (blue) and when applied field $F \approx 1.2 \text{ kVcm}^{-1}$ (dotted magenta), where at around of CQWs zone are similar.

In the next chapter, we expose the RAS experiments and their significance in the wonderful results of this work, following, is important to define and explain the role of the doping layer that as can see may be generated a significant intrinsic field which in contrast with the RAS results and our model the built-in electric field doesn't significatively important in the symmetry breaking ($D_2 \rightarrow C_{2v}$). Therefore, we calculate the possible conduction band bending due to the built-in electric field as can see in Figure 3.18.

We have taken into account a total structure width with an n-type doped layer, we remember that the high doping and large width can cause the calculations doesn't converge by this we implemented a damping factor to accelerate the convergence, also we calculated a potential profile considering an external electric field applied around of $F \approx 1.2 \text{ kVcm}^{-1}$. The results show that practically the total V_p and electric field (line-shape and magnitude) are kept as shown in Figure 3.17, if we compare the potential profiles V_p and V_F as see in Figure 3.18, it can observe that practically the band bending which is generated by electric field so much as by doped layer, as an external field applied are very similar if the external potential is around of $F \approx 1.2 \text{ kVcm}^{-1}$. This means that, if exists an electric field but is

comparable with surface field [97], hence is a small field. Therefore, we can say that the effects of the trions are associated with the asymmetry of the QWs as before mentioned.

3.2.2.2 The PR summary

In conclusion, the PR remains a powerful tool for experimental solid-state physics, especially in semiconductors study the facility to implement it, and the great information which gives as about fundamental transitions that in comparison with other spectroscopy is still better. Along with the experimental work, we could notice that the PR has the capability of detect behaviors which doesn't common in this spectroscopy as trions measured, and although this work is still in progress, the satisfaction to propound a novel source to study of an excitonic behavior as the trions, through easy spectroscopy without external perturbations. On the other side, the AQCWs has a large potential to study quantum phenomena, especially the interactions and process due to the exciton confined, in this case, something so simple as the relative widths in the CQWs generates a surprising behavior. rcode

3.2.3 Reflectance Anisotropy Spectroscopy (RAS)

THE RAS is the experimental tool that completes the set in this work, without the intention of replicates the physical background and interpretations about RAS, we focus on specific terms to detail our great results. This spectroscopy, is a powerful tool in the studying of semiconductors physics, being characterized as default anisotropy study tool. This experimental technique, was developed by Aspnes [67, 98, 99] to measure *surface-induced* optical anisotropy in cubic semiconductors, although this can be applied around of near-band-edge [100]. So, to our purposes, RAS is an excellent experimental tool to study optical anisotropies in CQWs structures.

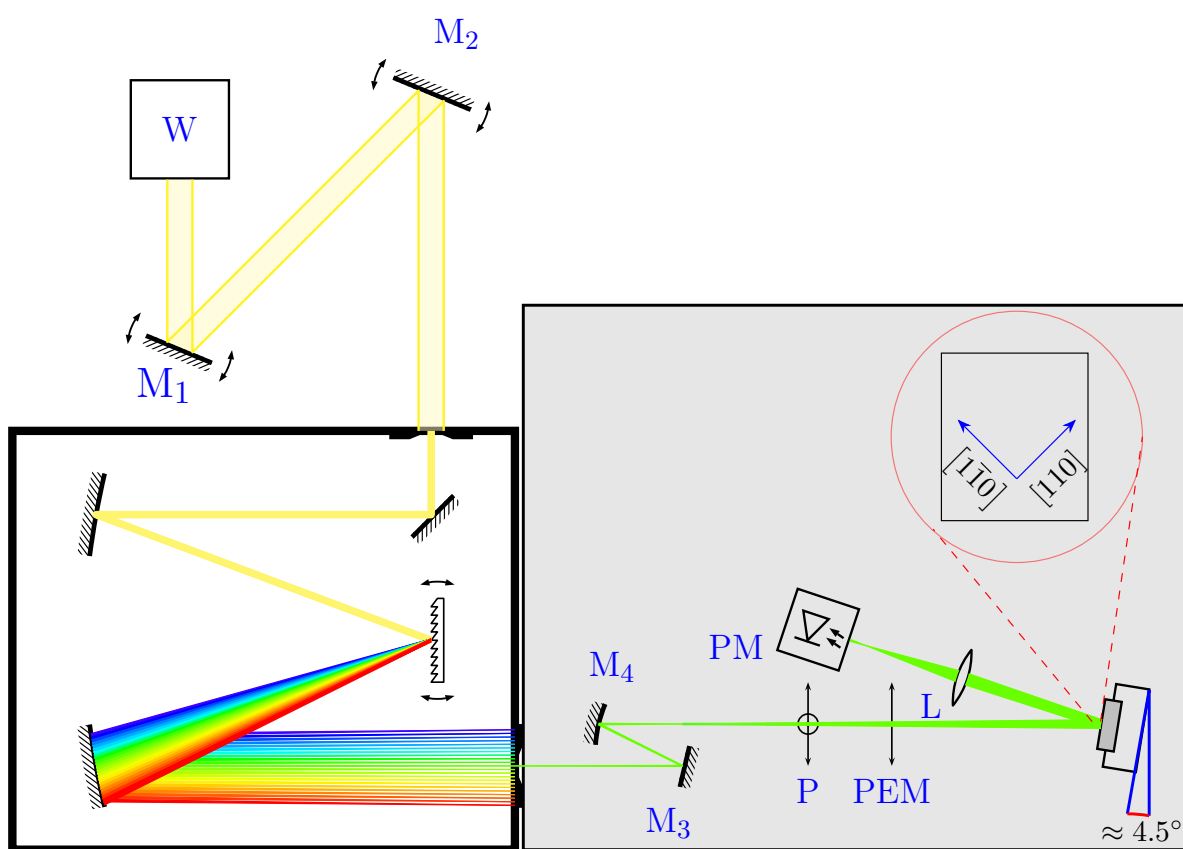


Figure 3.19

4

CONCLUSIONS

In this chapter raise the principal conclusion of this work and present the future experiments on these structures in the wake of obtained results.

BIBLIOGRAPHY

- [1] Mark Fox. Optical properties of solids, 2002. (Cited on pages II, 6, 7, 8, and 13.)
- [2] Kanchana Sivalertporn. Effect of barrier width on the exciton states in coupled quantum wells in an applied electric field. *Physics Letters A*, 380(22):1990–1994, 2016. (Cited on pages IV, 43, and 47.)
- [3] Nacer Debbar, Songcheol Hong, Jasprit Singh, Pallab Bhattacharya, and Rajeshwar Sahai. Coupled gaas/algaas quantum-well electroabsorption modulators for low-electric-field optical modulation. *Journal of Applied Physics*, 65(1):383–385, 1989. (Cited on pages IV and 47.)
- [4] Nikolai V Tkachenko. *Optical spectroscopy: methods and instrumentations*. Elsevier, 2006. (Cited on pages V and 28.)
- [5] Ask Hjorth Larsen, Jens Jørgen Mortensen, Jakob Blomqvist, Ivano E Castelli, Rune Christensen, Marcin Dułak, Jesper Friis, Michael N Groves, Bjørk Hammer, Cory Hargus, Eric D Hermes, Paul C Jennings, Peter Bjerre Jensen, James Kermode, John R Kitchin, Esben Leonhard Kolsbjerger, Joseph Kubal, Kristen Kaasbjerger, Steen Lysgaard, Jón Bergmann Maronsson, Tristan Maxson, Thomas Olsen, Lars Pastewka, Andrew Peterson, Carsten Rostgaard, Jakob Schiøtz, Ole Schütt, Mikkel Strange, Kristian S Thygesen, Tejs Vegge, Lasse Vilhelmsen, Michael Walter, Zhenhua Zeng, and Karsten W Jacobsen. The atomic simulation environment—a python library for working with atoms. *Journal of Physics: Condensed Matter*, 29(27):273002, 2017. (Cited on page VII.)
- [6] D Alonso-Álvarez, T Wilson, P Pearce, M Führer, D Farrell, and N Ekins-Daukes. Solcore: a multi-scale, python-based library for modelling solar cells and semiconductor materials. *Journal of Computational Electronics*, 17(3):1099–1123, 2018. (Cited on pages VII and 33.)
- [7] H. Hebal, Z. Koziol, S.B. Lisesivdin, and R. Steed. General-purpose open-source 1d self-consistent schrödinger-poisson solver: Aestimo 1d. *Computational Materials Science*, 186:110015, 2021. (Cited on pages VII and 48.)
- [8] Koichi Momma and Fujio Izumi. it VESTA3 for three-dimensional visualization of crystal, volumetric and morphology data. *Journal of Applied Crystallography*, 44(6):1272–1276, Dec 2011. (Cited on page VII.)
- [9] Till Tantau. Pgf/tikz, 2007. (Cited on page VII.)

- [10] MANI SUNDARAM, SCOTT A. CHALMERS, PETER F. HOPKINS, and ARTHUR C. GOSSARD. New quantum structures. *Science*, 254(5036):1326–1335, 1991. (Cited on page 2.)
- [11] Joachim Piprek. *Handbook of Optoelectronic Device Modeling and Simulation: Fundamentals, Materials, Nanostructures, LEDs, and Amplifiers*, Vol. 1. CRC Press, 2017. (Cited on pages 2, 3, and 5.)
- [12] Henri Alloul. *Introduction to the Physics of Electrons in Solids*. Springer Science & Business Media, 2010. (Cited on page 2.)
- [13] Manuel Cardona and Y Yu Peter. *Fundamentals of semiconductors*, volume 619. Springer, 2005. (Cited on pages 2, 7, 11, and 19.)
- [14] Karl W Böer and Udo W Pohl. *Semiconductor physics*. Springer, 2018. (Cited on page 3.)
- [15] Igor Vurgaftman, Matthew P Lumb, and Jerry R Meyer. *Bands and Photons in III-V Semiconductor Quantum Structures*, volume 25. Oxford University Press, 2020. (Cited on page 4.)
- [16] P. Vogl, Harold P. Hjalmarson, and John D. Dow. A semi-empirical tight-binding theory of the electronic structure of semiconductors†. *Journal of Physics and Chemistry of Solids*, 44(5):365–378, 1983. (Cited on pages 6 and 20.)
- [17] Rick Muller. Tight binding program to compute the band structure of simple semiconductors., 2017. (Cited on page 6.)
- [18] Jason Leonard. *Exciton Transport Phenomena in GaAs Coupled Quantum Wells*. Springer, 2017. (Cited on page 8.)
- [19] Paul Harrison and Alex Valavanis. *Quantum wells, wires and dots: theoretical and computational physics of semiconductor nanostructures*. John Wiley & Sons, 2016. (Cited on pages 10, 11, 13, and 14.)
- [20] Wolfgang Pauli. Über den Zusammenhang des Abschlusses der Elektronengruppen im Atom mit der Komplexstruktur der Spektren. *Zeitschrift für Physik*, 31(1):765–783, 1925. (Cited on page 11.)
- [21] S.L. Chuang. *Physics of Optoelectronic Devices*. Wiley Series in Pure and Applied Optics. Wiley, 1995. (Cited on page 13.)
- [22] Jasprit Singh. *Electronic and Optoelectronic Properties of Semiconductor Structures*. Cambridge University Press, 2003. (Cited on page 13.)
- [23] Gerald Bastard. *Wave mechanics applied to semiconductor heterostructures*. Wiley, 1990. (Cited on pages 13 and 49.)

- [24] John H Davies. *The physics of low-dimensional semiconductors: an introduction.* Cambridge university press, 1998. (Cited on page 13.)
- [25] Luis De La Peña. *Introducción a la mecánica cuántica.* Fondo de Cultura económica, 2014. (Cited on page 13.)
- [26] David J Griffiths and Darrell F Schroeter. *Introduction to quantum mechanics.* Cambridge University Press, 2018. (Cited on page 13.)
- [27] Jun John Sakurai and Eugene D Commins. *Modern quantum mechanics, revised edition,* 1995. (Cited on page 13.)
- [28] Claude Cohen-Tannoudji, Bernard Diu, and Franck Laloë. *Quantum Mechanics, Volume 1: Basic Concepts, Tools, and Applications.* John Wiley & Sons, 2019. (Cited on page 13.)
- [29] Nicholas Rivera and Ido Kaminer. Light–matter interactions with photonic quasi-particles. *Nature Reviews Physics*, 2(10):538–561, 2020. (Cited on page 14.)
- [30] Bas C Van Fraassen. *Laws and symmetry.* Clarendon Press, 1989. (Cited on page 16.)
- [31] Richard C Powell. *Symmetry, group theory, and the physical properties of crystals,* volume 824. Springer, 2010. (Cited on pages 16 and 18.)
- [32] Kristopher Tapp. *Symmetry: A mathematical exploration.* Springer Nature, 2021. (Cited on page 16.)
- [33] John F Cornwell. *Group theory in physics: An introduction.* Academic press, 1997. (Cited on page 16.)
- [34] Ulrich Müller. *Symmetry relationships between crystal structures: applications of crystallographic group theory in crystal chemistry,* volume 18. OUP Oxford, 2013. (Cited on page 16.)
- [35] Charles Kittel and Paul McEuen. *Kittel’s Introduction to Solid State Physics.* John Wiley & Sons, 2018. (Cited on pages 16, 17, and 18.)
- [36] Jenö Sólyom. *Fundamentals of the Physics of Solids: Volume 1: Structure and Dynamics,* volume 1. Springer Science & Business Media, 2007. (Cited on page 16.)
- [37] Sanat K Chatterjee. *Crystallography and the World of Symmetry,* volume 113. Springer Science & Business Media, 2008. (Cited on pages 17 and 18.)
- [38] J.P. McKelvey. *Solid State and Semiconductor Physics.* A Harper international edition. Harper & Row, 1966. (Cited on page 18.)
- [39] Cécile Malgrange, Christian Ricolleau, and Michel Schlenker. *Symmetry and Physical Properties of Crystals.* Springer, 2014. (Cited on page 18.)

- [40] N.W. Ashcroft, A.N. W, N.D. Mermin, W. Ashcroft, D. Mermin, N.D. Mermin, and Brooks/Cole Publishing Company. *Solid State Physics*. HRW international editions. Holt, Rinehart and Winston, 1976. (Cited on page 18.)
- [41] Richard C. Powell. *Symmetry in Solids*, pages 1–24. Springer New York, New York, NY, 2010. (Cited on page 18.)
- [42] Mildred S Dresselhaus, Gene Dresselhaus, and Ado Jorio. *Group theory: application to the physics of condensed matter*. Springer Science & Business Media, 2007. (Cited on pages 19 and 20.)
- [43] R. H. Parmenter. Symmetry properties of the energy bands of the zinc blende structure. *Phys. Rev.*, 100:573–579, Oct 1955. (Cited on page 19.)
- [44] Paul N Butcher, Norman H March, and Mario P Tosi. *Crystalline semiconducting materials and devices*. Springer Science & Business Media, 2013. (Cited on page 19.)
- [45] G.L. Bir and G.E. Pikus. *Symmetry and Strain-induced Effects in Semiconductors*. A Halsted Press book. Wiley, 1974. (Cited on page 20.)
- [46] Walter A. Harrison. Bond-orbital model and the properties of tetrahedrally coordinated solids. *Phys. Rev. B*, 8:4487–4498, Nov 1973. (Cited on page 20.)
- [47] J. C. Slater and G. F. Koster. Simplified lcao method for the periodic potential problem. *Phys. Rev.*, 94:1498–1524, Jun 1954. (Cited on page 20.)
- [48] Katherine Brading, Elena Castellani, and Nicholas Teh. Symmetry and Symmetry Breaking. In Edward N. Zalta, editor, *The Stanford Encyclopedia of Philosophy*. Metaphysics Research Lab, Stanford University, Fall 2021 edition, 2021. (Cited on page 20.)
- [49] John Wilfred Orton and Tom Foxon. *Molecular beam epitaxy: a short history*. Oxford University Press, USA, 2015. (Cited on page 24.)
- [50] Marius Grundmann. *Physics of semiconductors*, volume 11. Springer, 2010. (Cited on page 24.)
- [51] M. Yuan, A. Hernández-Mínguez, K. Biermann, and P. V. Santos. Tunneling blockade and single-photon emission in gaas double quantum wells. *Phys. Rev. B*, 98:155311, Oct 2018. (Cited on pages 25 and 46.)
- [52] John Weiner and Frederico Nunes. *Light-matter interaction: physics and engineering at the nanoscale*. Oxford University Press, 2017. (Cited on page 27.)
- [53] A. Einstein. Über die von der molekularkinetischen theorie der wärme geforderte bewegung von in ruhenden flüssigkeiten suspendierten teilchen. *Annalen der Physik*, 322(8):549–560, 1905. (Cited on page 28.)

- [54] C. A. Bravo-Velazques. Sistema de fotoluminiscencia para caracterización de pozos cuánticos acoplados. Bachelor Thesis to obtain Engineering Physicist degree, 2 2020. (Cited on page 30.)
- [55] Juan Jimenez and Jens W Tomm. *Spectroscopic Analysis of optoelectronic semiconductors*, volume 202. Springer, 2016. (Cited on page 32.)
- [56] Wei Lu and Ying Fu. *Spectroscopy of Semiconductors*. Springer International Publishing, 2018. (Cited on page 32.)
- [57] David Warren Ball. *The basics of spectroscopy*, volume 49. Spie Press, 2001. (Cited on page 32.)
- [58] Wolfgang Demtr̄der. *Electrodynamics and Optics*. Springer Nature, 2019. (Cited on page 32.)
- [59] Jose Solé, Luisa Bausa, and Daniel Jaque. *An introduction to the optical spectroscopy of inorganic solids*. John Wiley & Sons, 2005. (Cited on page 32.)
- [60] H. Khmissi, L. Sfaxi, L. Bouzaïene, F. Saidi, H. Maaref, and C. Bru-Chevallier. Effect of carriers transfer behavior on the optical properties of inas quantum dots embedded in algaas/gaas heterojunction. *Journal of Applied Physics*, 107(7):074307, 2010. (Cited on page 35.)
- [61] J. Kundrotas, A. Čerškus, S. Ašmontas, G. Valušis, B. Sherlike, M. P. Halsall, M. J. Steer, E. Johannessen, and P. Harrison. Excitonic and impurity-related optical transitions in be δ -doped GaAs/AlAs multiple quantum wells: Fractional-dimensional space approach. *Phys. Rev. B*, 72:235322, Dec 2005. (Cited on page 35.)
- [62] Jasprit Singh, KK Bajaj, and S Chaudhuri. Theory of photoluminescence line shape due to interfacial quality in quantum well structures. *Applied physics letters*, 44(8):805–807, 1984. (Cited on page 36.)
- [63] F-Y Juang, Jasprit Singh, Pallab K Bhattacharya, K Bajema, and R Merlin. Field-dependent linewidths and photoluminescence energies in gaas/algaas multiquantum well modulators. *Applied physics letters*, 48(19):1246–1248, 1986. (Cited on page 36.)
- [64] J. Maluenda and P. M. Frijlink. Abrupt transitions in composition and doping profile in GaAs/Ga_{1-x}Al_xAs heterostructures by atmospheric pressure movpe. *Journal of Vacuum Science & Technology B: Microelectronics Processing and Phenomena*, 1(2):334–337, 1983. (Cited on page 36.)
- [65] B. V. Shanabrook, O. J. Glembocki, and W. T. Beard. Photoreflectance modulation mechanisms in gaas-al_xga_{1-x}as multiple quantum wells. *Phys. Rev. B*, 35:2540–2543, Feb 1987. (Cited on page 37.)

- [66] B. O. Seraphin and D. E. Aspnes. Electric field effects in optical and first-derivative modulation spectroscopy. *Phys. Rev. B*, 6:3158–3160, Oct 1972. (Cited on page 37.)
- [67] DE Aspnes and DD Sell. Surface field effects in reflectance and first-derivative modulation spectra. *Solid State Communications*, 13(5):519–522, 1973. (Cited on pages 37 and 51.)
- [68] J Misiewicz, G Sek, and P Sitarek. Photoreflectance spectroscopy applied to semiconductors and semiconductor heterostructures. *Optica Applicata*, 29(3):327–363, 1999. (Cited on pages 37, 38, and 39.)
- [69] Michael Sydor, James Angelo, Jerome J. Wilson, W. C. Mitchel, and M. Y. Yen. Photoreflectance from gaas and gaas/gaas interfaces. *Phys. Rev. B*, 40:8473–8484, Oct 1989. (Cited on page 37.)
- [70] W. M. Theis, G. D. Sanders, C. E. Leak, K. K. Bajaj, and H. Morkoc. Excitonic transitions in gaas/ga_xal_{1-x}as quantum wells observed by photoreflectance spectroscopy: Comparison with a first-principles theory. *Phys. Rev. B*, 37:3042–3051, Feb 1988. (Cited on page 37.)
- [71] W. M. Theis, G. D. Sanders, K. R. Evans, L. L. Liou, C. E. Leak, K. K. Bajaj, C. E. Stutz, R. L. Jones, and Yia-Chung Chang. Extrinsic contributions to photoreflectance of al_xga_{1-x}as/gaas quantum wells: An investigation of the “donor-related” feature. *Phys. Rev. B*, 39:11038–11043, May 1989. (Cited on page 37.)
- [72] I Gontijo, YS Tang, RM De La Rue, CM Sotomayor Torres, JS Roberts, and JH Marsh. Photoreflectance and photoluminescence of partially intermixed gaas/algaas double quantum wells. *Journal of applied physics*, 76(9):5434–5438, 1994. (Cited on page 37.)
- [73] H. Shen and M. Dutta. Franz–keldysh oscillations in modulation spectroscopy. *Journal of Applied Physics*, 78(4):2151–2176, 1995. (Cited on page 39.)
- [74] R. Del Sole and D. E. Aspnes. Effect of surface and nonuniform fields in electroreflectance: Application to ge. *Phys. Rev. B*, 17:3310–3317, Apr 1978. (Cited on page 40.)
- [75] Manuel Cardona. Modulation spectroscopy. *Solid State Phys.*, 11, 1969. (Cited on page 41.)
- [76] B. O. Seraphin and N. Bottka. Band-structure analysis from electro-reflectance studies. *Phys. Rev.*, 145:628–636, May 1966. (Cited on page 41.)
- [77] A. M. Fox, D. A. B. Miller, G. Livescu, J. E. Cunningham, and W. Y. Jan. Excitonic effects in coupled quantum wells. *Phys. Rev. B*, 44:6231–6242, Sep 1991. (Cited on page 43.)

- [78] H. Shen, P. Parayanthal, F.H. Pollak, A.L. Smirl, J.N. Schulman, R.A. McFarlane, and I. D'Haenens. Observation of symmetry forbidden transitions in the room temperature photoreflectance spectrum of a gaas/gaalas multiple quantum well. *Solid State Communications*, 59(8):557–560, 1986. (Cited on page 43.)
- [79] H. Shen, X. C. Shen, Fred H. Pollak, and R. N. Sacks. Photoreflectance and photoreflectance-excitation spectroscopy of a gaas/ga_{0.67}al_{0.33}as multiple-quantum-well structure. *Phys. Rev. B*, 36:3487–3490, Aug 1987. (Cited on page 43.)
- [80] Z. M. Fang, A. Persson, and R. M. Cohen. Allowed 3h-1e transition in semiconductor quantum wells. *Phys. Rev. B*, 37:4071–4075, Mar 1988. (Cited on page 43.)
- [81] G. Bastard, E. E. Mendez, L. L. Chang, and L. Esaki. Exciton binding energy in quantum wells. *Phys. Rev. B*, 26:1974–1979, Aug 1982. (Cited on page 45.)
- [82] Y. Shinozuka and M. Matsuura. Wannier exciton in quantum wells. *Phys. Rev. B*, 28:4878–4881, Oct 1983. (Cited on page 45.)
- [83] K. Kheng, R. T. Cox, Merle Y. d' Aubigné, Franck Bassani, K. Saminadayar, and S. Tatarenko. Observation of negatively charged excitons x^- in semiconductor quantum wells. *Phys. Rev. Lett.*, 71:1752–1755, Sep 1993. (Cited on pages 45 and 48.)
- [84] Murray A. Lampert. Mobile and immobile effective-mass-particle complexes in nonmetallic solids. *Phys. Rev. Lett.*, 1:450–453, Dec 1958. (Cited on page 45.)
- [85] B. Stébé and A. Ainane. Ground state energy and optical absorption of excitonic trions in two dimensional semiconductors. *Superlattices and Microstructures*, 5(4):545–548, 1989. (Cited on page 45.)
- [86] P. Aceituno and A. Hernández-Cabrera. The role of excitons and trions on electron spin polarization in quantum wells. *Journal of Applied Physics*, 110(1):013724, 2011. (Cited on page 46.)
- [87] A. Manassen, E. Cohen, Arza Ron, E. Linder, and L. N. Pfeiffer. Exciton and trion spectral line shape in the presence of an electron gas in gaas/ala_s quantum wells. *Phys. Rev. B*, 54:10609–10613, Oct 1996. (Cited on pages 47 and 48.)
- [88] Gleb Finkelstein, Hadas Shtrikman, and Israel Bar-Joseph. Negatively and positively charged excitons in GaAs/al_xga_{1-x}As quantum wells. *Phys. Rev. B*, 53:R1709–R1712, Jan 1996. (Cited on pages 47 and 48.)
- [89] N N Sibeldin, M L Skorikov, and V A Tsvetkov. Formation of charged excitonic complexes in shallow quantum wells of undoped GaAs/AlGaAs structures under below-barrier and above-barrier photoexcitation. *Nanotechnology*, 12(4):591–596, nov 2001. (Cited on page 48.)

- [90] Israel Bar-Joseph. Trions in GaAs quantum wells. *Semiconductor Science and Technology*, 20(6):R29–R39, may 2005. (Cited on page 48.)
- [91] Christian Jirauschek and Tillmann Kubis. Modeling techniques for quantum cascade lasers. *Applied Physics Reviews*, 1(1):011307, 2014. (Cited on pages 48 and 49.)
- [92] Paul Harrison and Alex Valavanis. *Numerical solutions*, chapter 3, pages 81–130. John Wiley & Sons, Ltd, 2016. (Cited on page 48.)
- [93] L. R. Ram-Mohan, K. H. Yoo, and J. Moussa. The schrödinger–poisson self-consistency in layered quantum semiconductor structures. *Journal of Applied Physics*, 95(6):3081–3092, 2004. (Cited on page 48.)
- [94] Eric Cassan. On the reduction of direct tunneling leakage through ultrathin gate oxides by a one-dimensional schrödinger–poisson solver. *Journal of Applied Physics*, 87(11):7931–7939, 2000. (Cited on page 49.)
- [95] Yuji Ando and Tomohiro Itoh. Calculation of transmission tunneling current across arbitrary potential barriers. *Journal of Applied Physics*, 61(4):1497–1502, 1987. (Cited on page 49.)
- [96] V. D. Jovanović, D. Indjin, N. Vukmirović, Z. Ikonić, P. Harrison, E. H. Linfield, H. Page, X. Marcadet, C. Sirtori, C. Worrall, H. E. Beere, and D. A. Ritchie. Mechanisms of dynamic range limitations in GaAs/AlGaAs quantum-cascade lasers: Influence of injector doping. *Applied Physics Letters*, 86(21):211117, 2005. (Cited on page 49.)
- [97] A. Lastras-Martínez, R. E. Balderas-Navarro, L. F. Lastras-Martínez, and M. A. Vidal. Model for the linear electro-optic reflectance-difference spectrum of gaas(001) around E_1 and $E_1 + \Delta_1$. *Phys. Rev. B*, 59:10234–10239, Apr 1999. (Cited on page 51.)
- [98] D. E. Aspnes and A. A. Studna. Anisotropies in the above-band-gap optical spectra of cubic semiconductors. *Phys. Rev. Lett.*, 54:1956–1959, Apr 1985. (Cited on page 51.)
- [99] D. E. Aspnes. Above-bandgap optical anisotropies in cubic semiconductors: A visible–near ultraviolet probe of surfaces. *Journal of Vacuum Science & Technology B: Microelectronics Processing and Phenomena*, 3(5):1498–1506, 1985. (Cited on page 51.)
- [100] Su-Huai Wei and Alex Zunger. Theory of reflectance-difference spectroscopy in ordered iii-v semiconductor alloys. *Phys. Rev. B*, 51:14110–14114, May 1995. (Cited on page 51.)
- [101] Y. J. Chen, Emil S. Koteles, B. S. Elman, and C. A. Armiento. Effect of electric fields on excitons in a coupled double-quantum-well structure. *Phys. Rev. B*, 36:4562–4565, Sep 1987. (Not cited.)

- [102] D. A. B. Miller, D. S. Chemla, T. C. Damen, A. C. Gossard, W. Wiegmann, T. H. Wood, and C. A. Burrus. Band-edge electroabsorption in quantum well structures: The quantum-confined stark effect. *Phys. Rev. Lett.*, 53:2173–2176, Nov 1984. (Not cited.)
- [103] B. Koopmans, B. Koopmans, P.V. Santos, P.V. Santos, and M. Cardona. Microscopic reflection difference spectroscopy on semiconductor nanostructures. *physica status solidi (a)*, 170(2):307–315, 1998. (Not cited.)
- [104] Olivier Krebs and Paul Voisin. Giant optical anisotropy of semiconductor heterostructures with no common atom and the quantum-confined pockels effect. *Phys. Rev. Lett.*, 77:1829–1832, Aug 1996. (Not cited.)
- [105] Y. H. Chen, X. L. Ye, J. Z. Wang, Z. G. Wang, and Z. Yang. Interface-related in-plane optical anisotropy in $\text{gaas}/\text{al}_x\text{ga}_{1-x}\text{As}$ single-quantum-well structures studied by reflectance difference spectroscopy. *Phys. Rev. B*, 66:195321, Nov 2002. (Not cited.)
- [106] Wolfgang Braun, Achim Trampert, Lutz Däweritz, and Klaus H. Ploog. Nonuniform segregation of ga at alas/gaas heterointerfaces. *Phys. Rev. B*, 55:1689–1695, Jan 1997. (Not cited.)
- [107] C. G. Tang, Y. H. Chen, B. Xu, X. L. Ye, and Z. G. Wang. Well-width dependence of in-plane optical anisotropy in (001) $\text{gaas}/\text{algaas}$ quantum wells induced by in-plane uniaxial strain and interface asymmetry. *Journal of Applied Physics*, 105(10):103108, 2009. (Not cited.)
- [108] Yuan Li, Fengqi Liu, Xiaoling Ye, Yu Liu, Jiawei Wang, and Yonghai Chen. Quantitative investigation of intrinsic shear strain and asymmetric interface conditions in semiconductor superlattices. *Journal of Applied Physics*, 126(6):065704, 2019. (Not cited.)
- [109] J. L. Yu, S. Y. Cheng, Y. F. Lai, Q. Zheng, Y. H. Chen, and C. G. Tang. Tuning of in-plane optical anisotropy by inserting ultra-thin inas layer at interfaces in (001)-grown $\text{gaas}/\text{algaas}$ quantum wells. *Journal of Applied Physics*, 117(1):015302, 2015. (Not cited.)
- [110] Y.P. Varshni. Temperature dependence of the energy gap in semiconductors. *Physica*, 34(1):149–154, 1967. (Not cited.)
- [111] Omer Donmez, Ferhat Nutku, Ayse Erol, Cetin M. Arikan, and Yuksel Ergun. A study of photomodulated reflectance on staircase-like, n-doped $\text{gaas}/\text{alxga}_{1-x}\text{as}$ quantum well structures. *Nanoscale Research Letters*, 7(1):622, 2012. (Not cited.)
- [112] Sadao Adachi. *Properties of semiconductor alloys: group-IV, III-V and II-VI semiconductors*, volume 28. John Wiley & Sons, 2009. (Not cited.)

- [113] L. W. Molenkamp, R. Eppenga, G. W. 't Hooft, P. Dawson, C. T. Foxon, and K. J. Moore. Determination of valence-band effective-mass anisotropy in gaas quantum wells by optical spectroscopy. *Phys. Rev. B*, 38:4314–4317, Aug 1988. (Not cited.)
- [114] Ronald L. Greene, Krishan K. Bajaj, and Dwight E. Phelps. Energy levels of wannier excitons in GaAs – $ga_{1-x}al_xAs$ quantum-well structures. *Phys. Rev. B*, 29:1807–1812, Feb 1984. (Not cited.)
- [115] L. F. Lastras-Martínez, A. Lastras-Martínez, and R. E. Balderas-Navarro. A spectrometer for the measurement of reflectance-difference spectra. *Review of Scientific Instruments*, 64(8):2147–2152, 1993. (Not cited.)
- [116] Yutaka Takahashi, Yoshimine Kato, Satoru S. Kano, Susumu Fukatsu, Yasuhiro Shiraki, and Ryoichi Ito. The effect of electric field on the excitonic states in coupled quantum well structures. *Journal of Applied Physics*, 76(4):2299–2305, 1994. (Not cited.)
- [117] Chihiro Hamaguchi. *Basic Semiconductor Physics*. Springer International Publishing, 2017. (Not cited.)
- [118] I. Vurgaftman, J. R. Meyer, and L. R. Ram-Mohan. Band parameters for iii–v compound semiconductors and their alloys. *Journal of Applied Physics*, 89(11):5815–5875, 2001. (Not cited.)
- [119] J. M. Luttinger. Quantum theory of cyclotron resonance in semiconductors: General theory. *Phys. Rev.*, 102:1030–1041, May 1956. (Not cited.)
- [120] Lok C. Lew Yan Voon and Morten Willatzen. *Heterostructures: Basic Formalism*, pages 273–362. Springer Berlin Heidelberg, Berlin, Heidelberg, 2009. (Not cited.)
- [121] E. L. Ivchenko and S. D. Ganichev. *Spin-Photogalvanics*, pages 245–277. Springer Berlin Heidelberg, Berlin, Heidelberg, 2008. (Not cited.)
- [122] M.M. Glazov. *Electron & Nuclear Spin Dynamics in Semiconductor Nanostructures*. Series on Semiconductor Scienc. OXFORD University Press, 2018. (Not cited.)
- [123] D. J. BenDaniel and C. B. Duke. Space-charge effects on electron tunneling. *Phys. Rev.*, 152:683–692, Dec 1966. (Not cited.)
- [124] E. L. Ivchenko, A. Yu. Kaminski, and U. Rössler. Heavy-light hole mixing at zinc-blende (001) interfaces under normal incidence. *Phys. Rev. B*, 54:5852–5859, Aug 1996. (Not cited.)
- [125] Anubhav Jain, Shyue Ping Ong, Geoffroy Hautier, Wei Chen, William Davidson Richards, Stephen Dacek, Shreyas Cholia, Dan Gunter, David Skinner, Gerbrand Ceder, and Kristin a. Persson. The Materials Project: A materials genome approach to accelerating materials innovation. *APL Materials*, 1(1):011002, 2013. (Not cited.)

- [126] Wei Lu and Ying Fu. *Photoluminescence*, pages 107–158. Springer International Publishing, Cham, 2018. (Not cited.)
- [127] Heinz Kalt and Claus F Klingshirn. *Semiconductor Optics 1: Linear Optical Properties of Semiconductors*. Springer Nature, 2019. (Not cited.)
- [128] H. Kawai, K. Kaneko, and N. Watanabe. Photoluminescence of algaas/gaas quantum wells grown by metalorganic chemical vapor deposition. *Journal of Applied Physics*, 56(2):463–467, 1984. (Not cited.)
- [129] RW Keyes. Is quantum computing with solid state devices possible? *Applied Physics A*, 76(5):737–741, 2003. (Not cited.)
- [130] Geun-Hyeong Kim, Hyun-Jun Jo, Jong Su Kim, In-Ho Bae, Sang Jun Lee, et al. Optically biased photoreflectance spectroscopy of a gaas epitaxial layer and an algaas/gaas quantum well. *Current Applied Physics*, 15(10):1226–1229, 2015. (Not cited.)
- [131] David E Aspnes. Third-derivative modulation spectroscopy with low-field electroreflectance. *Surface science*, 37:418–442, 1973. (Not cited.)
- [132] Fred H Pollak. Modulation spectroscopy of semiconductors and semiconductor microstructures. *Handbook on Semiconductors*, 2:527–635, 1994. (Not cited.)
- [133] R. Kudrawiec and J. Misiewicz. Photoreflectance and contactless electroreflectance measurements of semiconductor structures by using bright and dark configurations. *Review of Scientific Instruments*, 80(9):096103, 2009. (Not cited.)
- [134] Kelin J. Kuhn, Cheng Juang, and Robert B. Darling. An enhanced and linear stark shift in $n - i - n$ algaas/gaas symmetric and asymmetric coupled quantum wells. *Journal of Applied Physics*, 69(5):3135–3141, 1991. (Not cited.)
- [135] Xuejun Zhu, P. B. Littlewood, Mark S. Hybertsen, and T. M. Rice. Exciton condensate in semiconductor quantum well structures. *Phys. Rev. Lett.*, 74:1633–1636, Feb 1995. (Not cited.)
- [136] Michael Stern, Vladimir Umansky, and Israel Bar-Joseph. Exciton liquid in coupled quantum wells. *Science*, 343(6166):55–57, 2014. (Not cited.)
- [137] J. Feldmann, G. Peter, E. O. Göbel, P. Dawson, K. Moore, C. Foxon, and R. J. Elliott. Linewidth dependence of radiative exciton lifetimes in quantum wells. *Phys. Rev. Lett.*, 59:2337–2340, Nov 1987. (Not cited.)
- [138] M. T. Portella-Oberli, V. Ciulin, J. H. Berney, B. Deveaud, M. Kutrowski, and T. Wojtowicz. Interacting many-body systems in quantum wells: Evidence for exciton-trion-electron correlations. *Phys. Rev. B*, 69:235311, Jun 2004. (Not cited.)

- [139] K. Sivalertporn, L. Mouchliadis, A. L. Ivanov, R. Philp, and E. A. Muljarov. Direct and indirect excitons in semiconductor coupled quantum wells in an applied electric field. *Phys. Rev. B*, 85:045207, Jan 2012. (Not cited.)
- [140] D. J. Chadi and M. L. Cohen. Tight-binding calculations of the valence bands of diamond and zincblende crystals. *physica status solidi (b)*, 68(1):405–419, 1975. (Not cited.)
- [141] Kristin Persson. Materials data on gaas (sg:216) by materials project, 11 2014. An optional note. (Not cited.)
- [142] Marvin L Cohen and James R Chelikowsky. *Electronic structure and optical properties of semiconductors*, volume 75. Springer Science & Business Media, 2012. (Not cited.)
- [143] Tsuneya Ando, Alan B. Fowler, and Frank Stern. Electronic properties of two-dimensional systems. *Rev. Mod. Phys.*, 54:437–672, Apr 1982. (Not cited.)
- [144] M G Burt. The justification for applying the effective-mass approximation to microstructures. *Journal of Physics: Condensed Matter*, 4(32):6651–6690, aug 1992. (Not cited.)
- [145] Jenö Sólyom. *Fundamentals of the Physics of Solids: Volume II: Electronic Properties*, volume 2. Springer Science & Business Media, 2008. (Not cited.)
- [146] Jenö Sólyom. *Fundamentals of the Physics of Solids: Volume 3-Normal, Broken-Symmetry, and Correlated Systems*, volume 3. Springer Science & Business Media, 2010. (Not cited.)
- [147] Warren James Elder. *Semi-empirical modelling of SiGe hetero-structures*. PhD dissertation, Imperial College London, 2012. (Not cited.)
- [148] Matthias Ehrhardt and Thomas Koprucki. *Multi-Band Effective Mass Approximations: Advanced Mathematical Models and Numerical Techniques*, volume 94. Springer, 2014. (Not cited.)